Research paper

Applying molecular hybridization to design a new class of pyrazolo[3,4-*d*] pyrimidines as Src inhibitors active in hepatocellular carcinoma

Salvatore Di Maria [a,1], Raffaele Passannanti [a,1], Federica Poggialini [a,1], Chiara Vagaggini [a], Alessia Serafinelli [a], Elena Bianchi [b], Paolo Governa [a], Lorenzo Botta [c,d], Giovanni Maga [b], Emmanuele Crespan [b], Fabrizio Manetti [a,c], Elena Dreassi [a], Francesca Musumeci [e,**], Anna Carbone [e,*], Silvia Schenone [e,f]

[a] *Department of Biotechnology, Chemistry, and Pharmacy, University of Siena, Via Aldo Moro 2, 53100, Siena, Italy*
[b] *Institute of Molecular Genetics (IGM), IGM-CNR, Via Abbiategrasso 207, I-27100, Pavia, Italy*
[c] *Lead Discovery Siena S.r.l., Via Vittorio Alfieri 31, I-53019, Castelnuovo Berardenga, Italy*
[d] *Department of Ecological and Biological Sciences, University of Tuscia, Largo Dell'Universita Snc, I-01100, Viterbo, Italy*
[e] *Department of Pharmacy, University of Genoa, Viale Benedetto XV 3, 16132, Genoa, Italy*
[f] *IRCCS Ospedale Policlinico San Martino, Genova, Largo Rosanna Benzi 10, 16132, Genoa, Italy*

ARTICLE INFO

ABSTRACT

Hepatocellular carcinoma (HCC) is the most common type of liver solid tumor and the second leading cause of cancer-related deaths worldwide. Although new treatment options have been recently approved, the development of tumor resistance and the poor prognosis for advanced HCC make the current standard of care unsatisfying. In this scenario, the non-receptor tyrosine kinase (TK) c-Src emerged as a promising target for developing new anti-HCC agents. Our group reported a large library of pyrazolo[3,4-*d*]pyrimidines active as potent c-Src inhibitors. Starting from these data, we applied a molecular hybridization approach to combine the *in-house* pyrazolo[3,4-*d*]pyrimidine SI192 with the approved TK inhibitor (TKI) dasatinib, with the aim of identifying a new generation of Src inhibitors. Enzymatic results prompted us to design second-generation compounds with a better binding profile based on a hit optimization protocol comprised of molecular modeling and on-paper rational design. This investigation led to the identification of a few nanomolar Src inhibitors active toward two HCC cell lines (HepG2 and HUH-7) selected according to their high and low c-Src expression, respectively. In particular, **7e** showed an IC_{50} value of 0.7 nM toward Src and a relevant antiproliferative efficacy on HepG2 cells after 72h ($IC_{50} = 2.47$ μM). Furthermore, **7e** exhibited a cytotoxic profile better than dasatinib. The ADME profile suggested that **7e** deserves further investigation as a promising TKI in cancer therapies. Finally, **7e**'s ability to inhibit HepG2 cell proliferation, elicit an irreversible cytotoxic effect, arrest cellular migration, and induce apoptotic-mediated cell death was assessed.

1. Introduction

Hepatocellular carcinoma is the most common type of liver solid tumor and the second leading cause of cancer-related deaths worldwide [1]. The treatment options are mainly represented by surgical resection, liver transplantation, or ablation for early-stage HCC patients, whereas systemic chemotherapy remains the main treatment for patients with advanced HCC who are not candidates for surgery [2]. Over the years,

various anticancer drugs have been used for the treatment of HCC, such as doxorubicin, cisplatin, and fluorouracil, but they recorded a 10 % response showing a low pharmacological impact and prompting the search for targeted approaches [3]. These studies led to the approval of a number of monoclonal antibodies and multi-kinase inhibitors in the last two decades [4,5]. Among kinase inhibitors, sorafenib **1** (Fig. 1) was the first compound to be approved (2007) by the US Food and Drug Administration (FDA) for systemic treatment of HCC and, till today,

---

* Corresponding author.
** Corresponding author.
E-mail addresses: francesca.musumeci@unige.it (F. Musumeci), anna.carbone1@unige.it (A. Carbone).
[1] These authors contributed equally.

remains a first-choice drug in patients with unresectable disease [6]. Since 2017, three additional multi-kinases inhibitors (namely, regorafenib **2**, lenvatinib **3**, and cabozantinib **4**, Fig. 1) have been approved by the FDA [7,8].

Despite these advancements, the development of tumor resistance and the 2-year median overall survival for advanced HCC make the current standard of care unsatisfying. Thus, the identification of novel compounds and combination regimens for chemotherapy is needed [2,9, 10]. Studies on the signaling pathways associated with HCC progression have unveiled the participation of additional kinases, such as the non-receptor TK Src.

Src, a kinase overexpressed in various cancers [11], exhibits high levels, particularly in the early stages of HCC. This heightened expression has been consistently associated with cancer progression as it stimulates cell proliferation and angiogenesis through focal adhesion kinase (FAK)-mediated pathways [12]. Based on this evidence, blocking Src emerged as a promising approach for identifying novel agents for HCC therapy. In particular, dasatinib **5** (Fig. 1) inhibits viability with a favorable median IC_{50} value in some HCC cell cultures [13]. It is worth noting that dasatinib is a dual inhibitor because it blocks not only Src but also Abl, another TK involved in HCC with IC_{50} values of 0.8 and 0.6 nM, respectively [14].

In our group, many efforts have been devoted to the synthesis of a large library of pyrazolo[3,4-*d*]pyrimidines decorated at N1, C4, and C6 positions to obtain potent c-Src and/or c-Abl inhibitors [15–17]. The X-ray crystallographic study of Src in complex with the *in-house* inhibitor SI192 **6** (Fig. 1) (K_i values of 210 and 150 nM toward Src and Abl, respectively) [18] allowed us to deeply understand the inhibitor-target interactions: the anilino NH group and the pyrazole N2 are involved in two hydrogen bonds with Thr338 and Met341, respectively.

Furthermore, the binding site presents an accessible hydrophobic pocket where bulky chains can enter and generate favorable ligand-protein interactions [19].

A powerful medicinal chemistry strategy entails the structural hybridization of clinically used drugs to generate new putative bioactive entities with higher probability rates, improved PK-related properties, and the ability to circumvent drug resistance. On this basis, herein we report the synthesis of a small library of new generation hybrid compounds between SI192 **6** and dasatinib **5**. Among them, the most promising derivatives were optimized by a protocol comprised of molecular modeling and on-paper rational design to increase their inhibitory activity toward the target, to ameliorate PK properties, and their usability as antitumor agents, in particular in HCC. As a result, **7e** emerged as the best compound that deserves additional investigation as a promising TKI in cancer therapies.

2. Results and discussion

To identify new Src inhibitors, the merge-hybridization of SI192 **6** with dasatinib **5** led to design **7a-c** (Fig. 2). SI192 **6** was selected as the starting point because previous studies showed that pyrazolo[3,4-*d*] pyrimidines bearing a C6 morpholinoethylthio chain possessed promising *in vitro* and *in vivo* activity in tumor models characterized by Src overexpression [19,20]. Then, we inserted the aminothiazole-carboxamide moiety, representing a portion of the central scaffold of dasatinib, as a linker between the C4 of the pyrazolo[3, 4-*d*]pyrimidine core and the phenyl ring, which was decorated with different functional groups. Finally, following a molecular simplification approach as a design strategy to shorten synthetic routes, the phenyl-ethyl side chain at the pyrazole N1 was replaced with a methyl group.
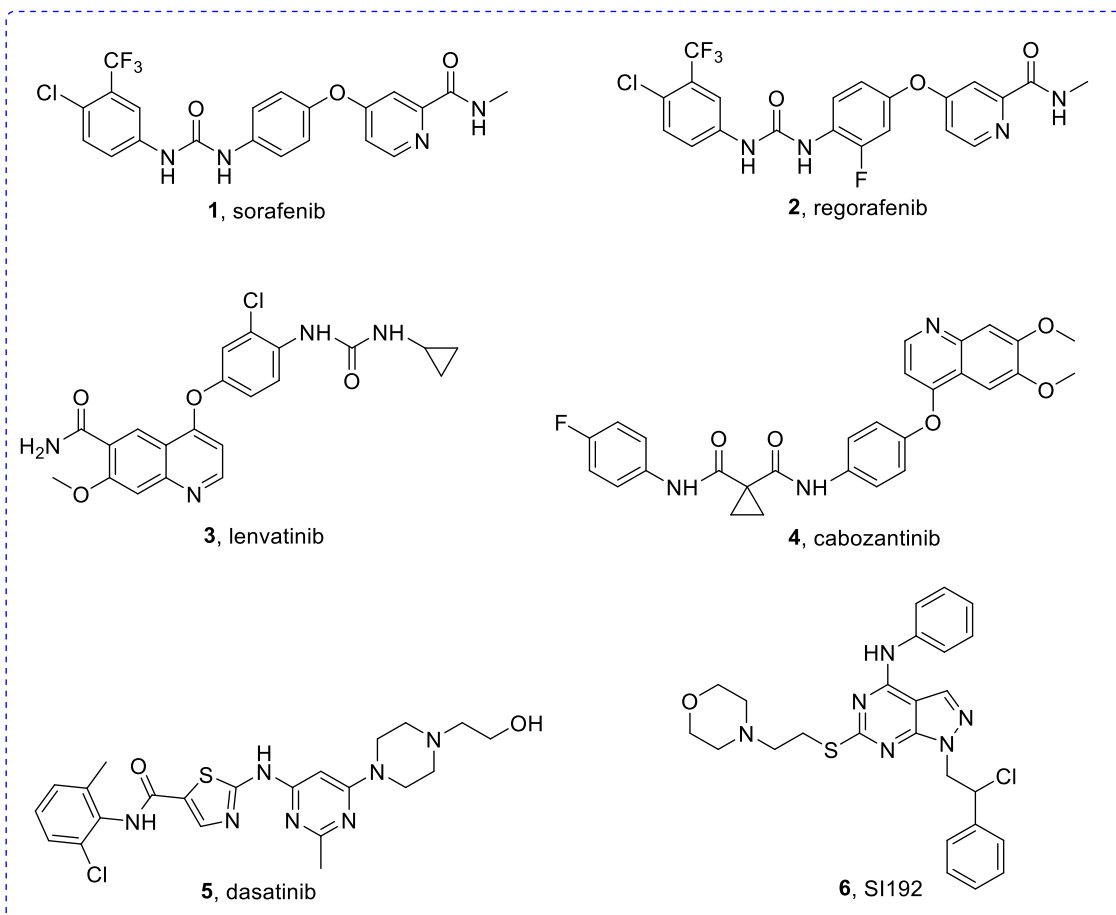

Fig. 1. Structures of approved TKIs sorafenib **1**, regorafenib **2**, lenvatinib **3**, cabozantinib **4**, and the dual Src/Abl inhibitors dasatinib **5** and SI192 **6**.
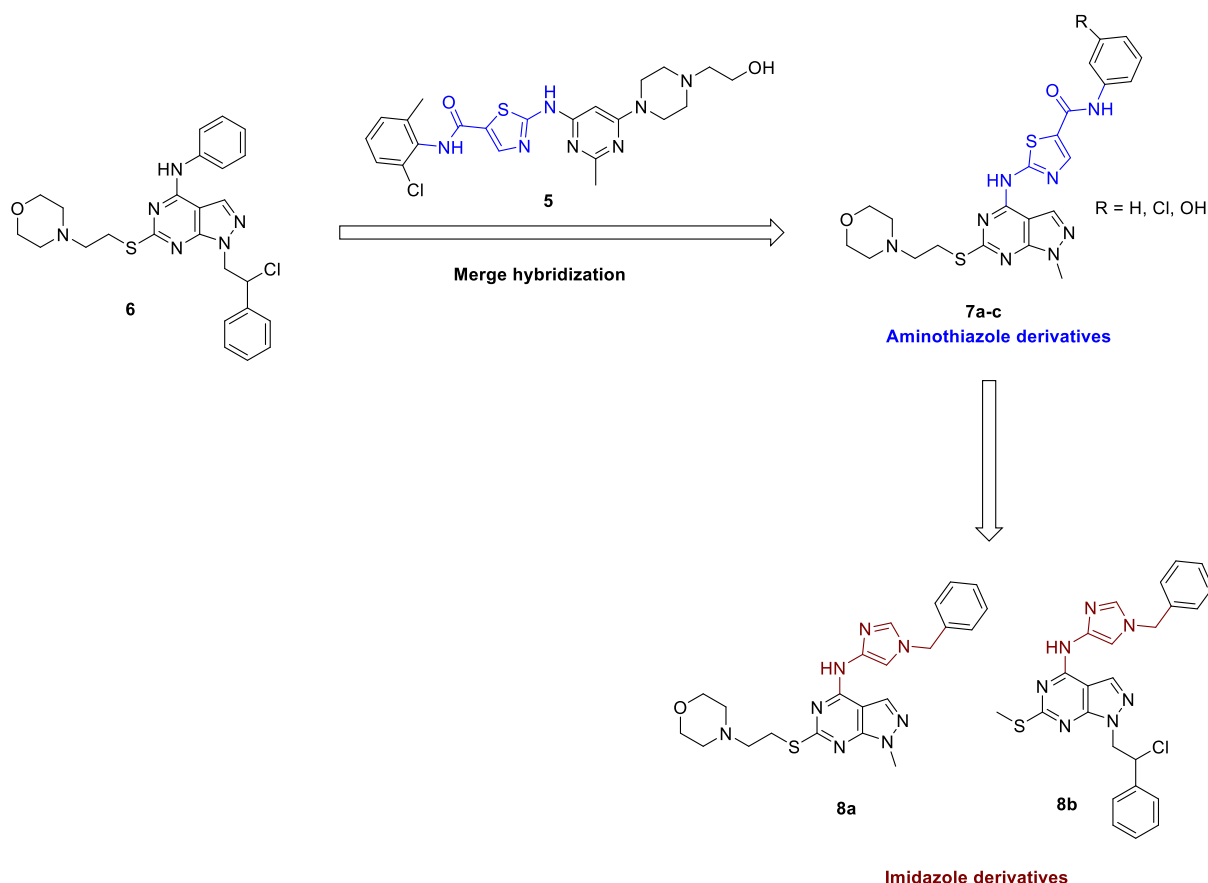
Fig. 2. Design of aminothiazole and imidazole derivatives as potential Src inhibitors.

We also designed and synthesized the imidazole derivatives **8a,b** (Fig. 2) to expand SAR analysis and increase the chances of finding new potent Src inhibitors based on the rationale that bioisosteres usually share a similar inhibitory profile [21]. Both **8a,b** show a simple methylene bridge instead of an amido group and an amino-imidazole ring instead of an amino-thiazole core at the C4. On the contrary, they differ for the N1 and C6 substituents: **8a**, analogously to **7a-c**, presents a N1 methyl group and a C6 morpholinoethylthio chain, whereas **8b** presents a N1 2-chloro-2-phenylethyl chain (introduced to increase lypophilicity and improve membrane permeability) and a C6 methylthio group.

Based on biological results, **7c** emerged as a promising Src inhibitor, showing an IC$_{50}$ = 24 nM. Furthermore, the antiproliferative activity of **7c** was assessed on the HepG2 cell line, which overexpresses c-Src., was evaluated. Despite its potent c-Src inhibition, **7c** affected to a moderate extent the HepG2 cell viability (IC$_{50}$ value > 50 μM) (see paragraph 2.3). For this reason, we performed an optimization study on **7c** by synthesizing **7d-h** (Fig. 3). In particular, to investigate how the modification of physicochemical properties of compounds (such as aqueous solubility and apparent permeability) may influence the biological activity, an on-paper rational design was applied and led to **7f-h**. On the other hand, **7d, e** were designed on the basis of suggestions taken from molecular modeling simulations that were performed for fine-tuning the inhibitor-Src interactions.

2.1. Molecular modeling simulations

Molecular docking and dynamics simulations were applied to predict the binding mode of **7c** on c-Src and to hypothesize which of the three possible conformational states of the kinase was preferred for binding (see Supporting Information) [22,23]. Results suggested that **7c** could stabilize the active conformation of Src, thus acting as a potential type I

kinase inhibitor. In a next step, the modelled complex between the active conformation of Src and **7c** was used to design second-generation compounds with a better binding profile, based on a hit optimization protocol comprised of affinity grid maps, molecular docking and dynamics simulations. As a result, a bromide or a methyl substituent at position 2 of the peripheral phenyl ring of **7c** was suggested to reinforce the inhibitor binding by hydrophobic interactions with the ATP binding site (Fig. 4). Molecular docking simulations showed that both the bromo and methyl analogues **7d** and **7e**, respectively, maintained the same binding pose of the parent compound, while GaMD simulations confirmed the stability of the corresponding complexes. Based on these results, both compounds were synthesized and tested for their ability to inhibit the Src kinase activity.

2.2. Chemistry

The class of pyrazolo[3,4-*d*]pyrimidine derivatives bearing a N1 methyl group and a C6 2-(4-morpholino)ethylthio moiety were obtained by introducing in C4 the desired chains previously synthesized (Schemes 1S,2S), as reported in Scheme 1. The preparation of intermediate **14** started from ethyl ethoxymethylenecyanoacetate **9** which was cyclized with methylhydrazine in refluxing ethanol to afford the pyrazole **10**. The reaction with benzoyl isothiocyanate and the subsequent cyclization of intermediate **11** in basic conditions gave the thione **12**, which was alkylated with 4-(2-chloroethyl)morpholine hydrochloride to obtain intermediate **13**. This latter compound was halogenated using the Vilsmeier-Haack reaction leading to the intermediate **14**, which was subsequently reacted with the appropriate synthons **15a-e** (Scheme 1S) by replacing the C4 chlorine atom. In detail, the synthesis of aminothiazole derivatives **7a-e** was optimized by testing different reaction conditions, since the desired results were not obtained by refluxing the
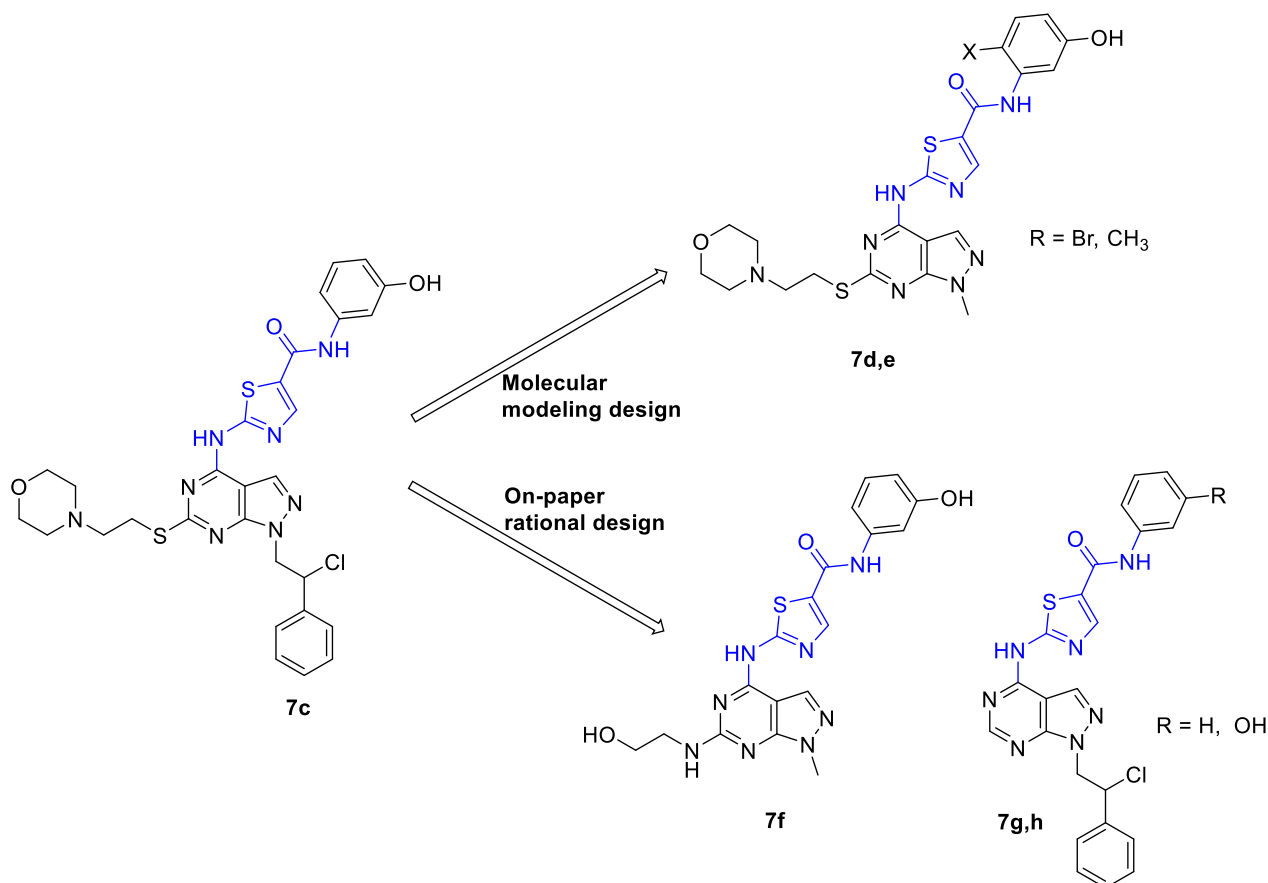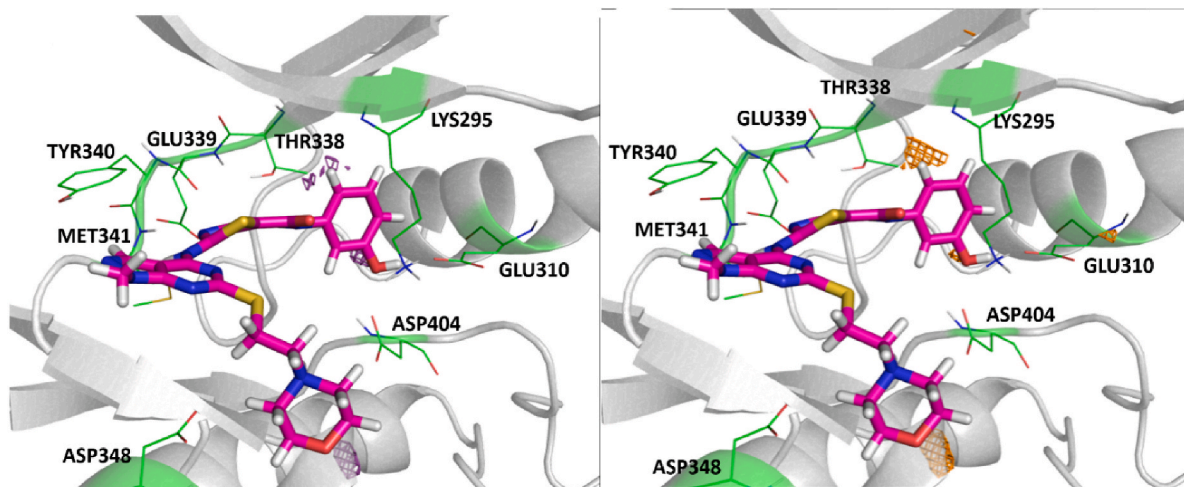
Fig. 3. Optimization study affording **7d-h**.

Fig. 4. Graphical representation of merging the predicted binding pose of **7c** within the ATP binding site and the affinity grid maps for bromine (left, purple) and aliphatic carbon (right, orange) atom probes, respectively. Based on these results, the bromo and methyl derivatives of **7c** were designed, synthesized, and assayed.

reaction mixture in ethanol. Neither the addition of a base (TEA) nor the change of solvent gave the desired compounds. Thus, the Buchwald reaction, known for its wide use in the coupling of aromatic amines, was chosen for the preparation of these derivatives. The reaction between **14** and **15a-e** gave **7a-e** in higher yield with Xantphos (45–70 %) in comparison to *t*-Bu-Xphos. Conversely, the synthesis of **8a** was accomplished by reacting **14** and **16** (Scheme 2S) in refluxing ethanol by adding a catalytic amount of TEA.

The synthesis of **7f** (Scheme 2) started from the alkylation of intermediate **12** with iodomethane to give **17**, which was halogenated

through Vilsmeier chlorination obtaining intermediate **18**. The subsequent Buchwald coupling between **15c** and **18**, using Xantphos as a ligand, was performed to give the methylthio intermediate **19**. The subsequent oxidation to sulfone using *m*-CPBA and the replacement with ethanolamine led to the desired compound **7f** (43 %).

C6 unsubstituted compounds **7g,h** bearing the N1 2-cloro-2-phenyl-ethyl chain were synthesized by Buchwald reaction between the intermediate **20a** and **15a,c** (Scheme 3) in good yields (48–57 %). The usual reaction conditions were adopted for the preparation of **8b** (yield 65 %), starting from intermediates **20b** and **16**, with the only modification of
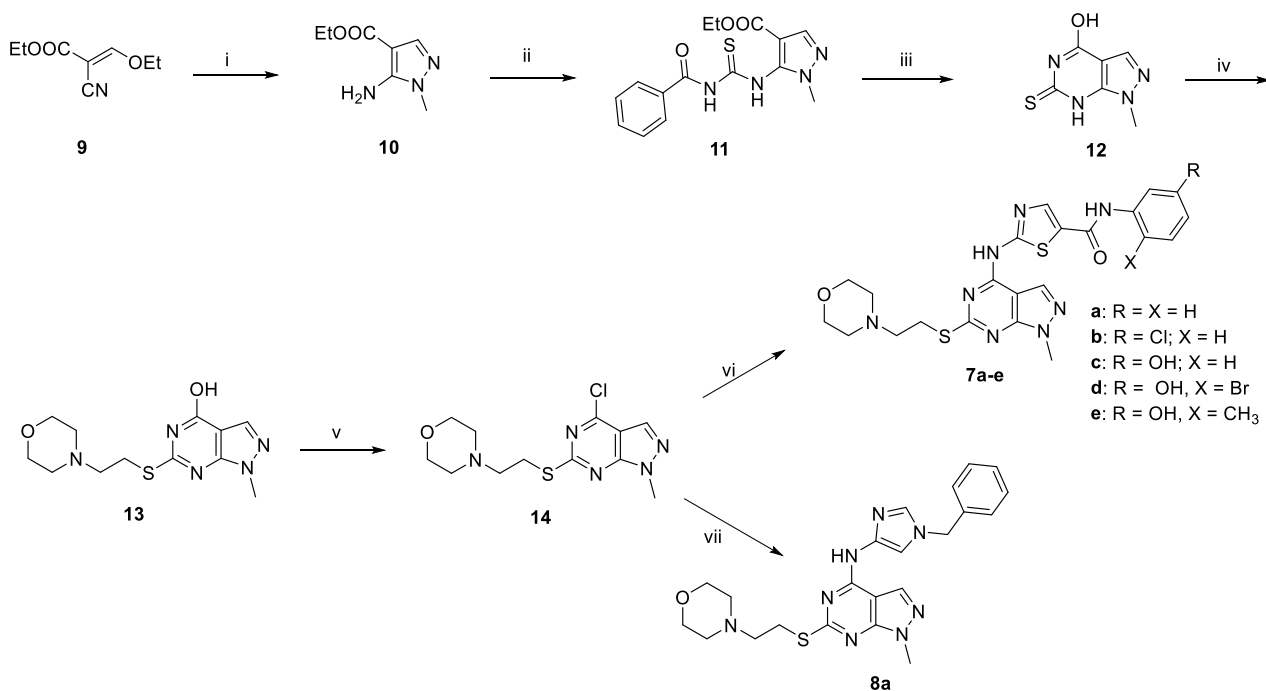
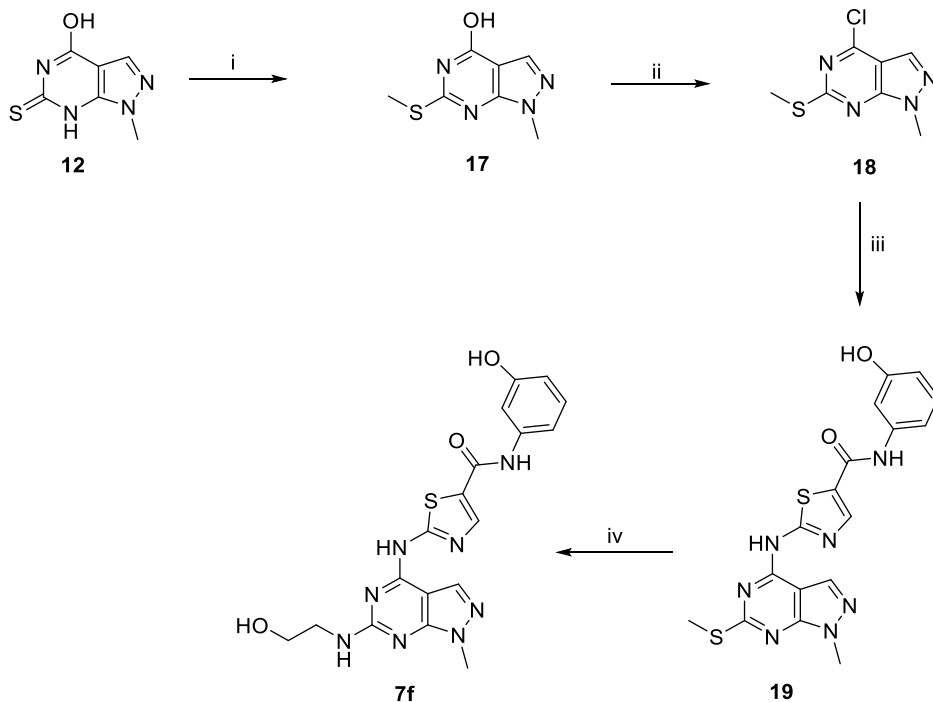**Scheme 1.** Synthesis of aminothiazoles **7a-e** and imidazole **8a**.
Reagents and conditions: i) methylhydrazine, EtOH, reflux, 8 h, 73 %; ii) benzoyl isothiocyanate, dry THF, reflux, 6 h, 85 %; iii) 2 N NaOH, reflux, 5 h, 88 %; iv) 4-(2-chloroethyl)morpholine hydrochloride, NaOH, EtOH, DMF, reflux, 8 h, 64 %; v) POCl$_3$, dry DMF, dry CHCl$_3$, reflux, 4 h, 55 %; vi) Pd$_2$(dba)$_3$, Xantphos, dry 1,4-dioxane, 30 min, rt; then **15a-e**, K$_2$CO$_3$, 4 h, reflux, 45–70 %; vii) **16**, TEA, EtOH, 8 h, reflux, 45 %.

adding fresh distilled TEA as a catalyst (Scheme 3).

2.3. Biological data

The aminothiazole derivatives **7a,c** showed significant c-Src

inhibition (Table 1), comparable to that of potent pyrazolo[3,4-*d*]pyrimidines previously reported [24]. In particular, the presence of a hydroxy group in the meta position of the aniline ring (**7c**) gave rise to an appreciable increase in the inhibitory activity compared to the unsubstituted analog **7a**. Therefore, a polar interaction between the OH group

Scheme 2. Synthesis of aminothiazole **7f**.
Reagents and conditions: i) iodomethane, dry THF, reflux, 12 h, 87 %; ii) POCl$_3$, dry DMF, dry CHCl$_3$, reflux, 4 h, 91 %; iii) Pd$_2$(dba)$_3$, Xantphos, dry 1,4-dioxane, 30 min, rt; then **15c**, K$_2$CO$_3$, 4 h, reflux, 82 %; iv) a) *m*-CPBA, dry DCM, dry DMF, rt, 2 h; b) ethanolamine, DMSO/butanol 1:2, reflux, 8 h, 43 %.
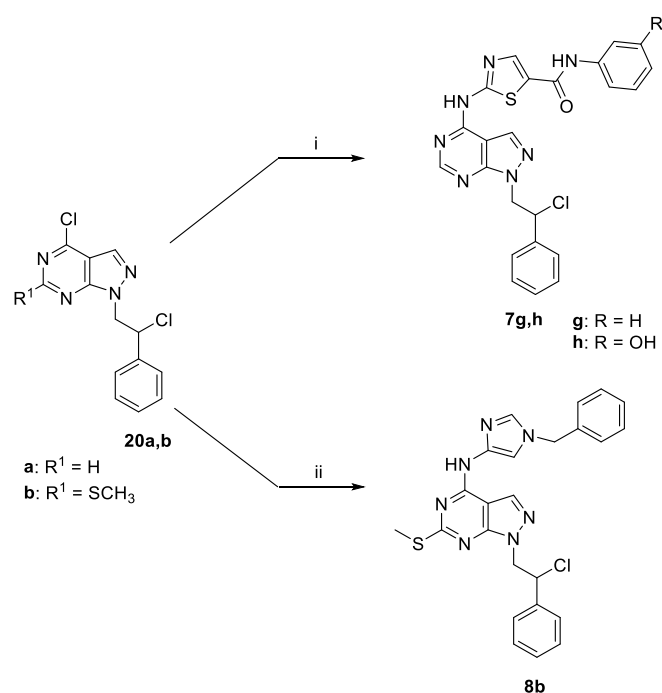
Scheme 3. Synthesis of aminothiazoles **7g,h** and imidazole **8b**.
Reagents and conditions: i) Pd$_2$(dba)$_3$, Xantphos, dry 1,4-dioxane, 30 min, rt; then **15a,c**, K$_2$CO$_3$, 4 h, reflux, 48–57 %; ii) **16**, TEA, EtOH, 6 h, reflux, 65 %.

and Glu310 of the c-Src kinase pocket can be envisioned, as previously described [19].

A low inhibitory effect on c-Src was exerted by imidazole derivatives **8a,b** (Table 1). As an example, **8a** is approximately ten-fold less active than the aminothiazole precursor **7a**, suggesting that the imidazole chain gave rise to weak interactions within the c-Src pocket.

Based on the obtained results, we further investigated the amino-thiazole class through the synthesis of additional derivatives **7d-h** designed to enhance the inhibitory potency toward c-Src and their ability to affect HepG2 cell viability.

Interestingly, the enzymatic assay (Table 1) confirmed the computational prediction for **7e** which was characterized by an activity (IC$_{50}$ = 0.7 nM) about 34-fold higher than that of **7c** (IC$_{50}$ = 24 nM), and comparable to that of dasatinib (20 nM). Differently, **7d** showed a significant decrease in inhibitory activity (IC$_{50}$ = 258 nM) compared to **7c**. Among the compounds obtained by on-paper rational design, only the pyrazolo-pyrimidine **7f** (IC$_{50}$ = 2.5 nM) resulted more active than **7c**.

Finally, the antiproliferative activity of **7a,c-h** was evaluated on two HCC cell lines: HepG2 and HUH-7 that were selected due to the high and low c-Src expression levels, respectively, as reported in The Human Protein Atlas [25–27]. As reported in Table 2, compounds **7d,e,h** showed a time-dependent antiproliferative activity, and all derivatives **7a,d-h** resulted more active than **7c** after 72 h of treatment on HepG2 cells. In detail, analysis of the cell activity at 24 h of incubation showed that **7d,e**, bearing two substituents on the aromatic ring of the benzamide moiety, showed higher cytotoxic activity (IC$_{50}$ = 12.02 μM and 59.64 μM, respectively) compared to the unsubstituted analog **7a** (IC$_{50}$ > 100 μM). Thus, the presence of a bromide (**7d**) rather than a methyl group (**7e**) on the phenyl ring resulted significantly interesting since induced a relevant cell death after just 24 h of incubation. The replacement of the C6 morpholine chain with the ethanolamine moiety (**7f**) and the mono-substitution with a hydroxyl group on the benzamide ring led to a loss of activity at 24 h (IC$_{50}$ > 100 μM).

Also the C6 unsubstituted derivatives **7g,h**, characterized by the presence of a N1 chlorophenylethyl chain, showed a low cell activity profile (IC$_{50}$ = 100 and 87.12 μM, respectively).

Moving to 48 h of treatment, **7d,e,g,h** improved their anti-proliferative activity (IC$_{50}$ from 5.06 to 13.89 μM), while **7a** and **7f** were inactive. After 72 h of treatment, all tested compounds induced a significant drop in HepG2 cell viability, with single-digit micromolar IC$_{50}$ values. In particular, **7d** and **7e** resulted the most promising derivatives possessing IC$_{50}$ values of 1.55 and 2.47 μM, respectively.

The same compounds in HUH-7 cells showed a similar trend of activity but higher IC$_{50}$ values (Table 2). In detail, at the lowest time point (24 h) **7a,f,g,h** confirmed the lack of action, **7d** doubled its IC$_{50}$ value, **7e** confirmed the activity, while exhibited a significant deterioration of efficacy at the longest time points (48,72 h), resulting in doubled or five-fold increased IC$_{50}$ values, respectively. This behaviour is probably due to the low HUH-7 physiological c-Src expression.

Compound **7e**, identified as the most promising derivative of the series, was further investigated for its cytotoxic profile by checking the activity on the healthy keratinocytes HaCaT and the embryonic HEK293 cell lines. HEK293 cells resulted more sensible than HaCaT to the effect of **7e**, resulting in CC$_{50}$ values among 18-5 μM from 24 to 72 h of treatment. However, the values obtained are generally found to be one order of magnitude higher than those obtained for dasatinib, used as reference. When the toxic profile of **7e** was checked on HaCaT, an acceptable safety profile was obtained at 24 and 48 h (CC$_{50}$s almost doubled than the corresponding IC$_{50}$s on HepG2 at the same time), while after 72 h the two parameters nearly equalized. As seen for the HEK293 cells, also in this case dasatinib still showed a more pronounced and relevant toxicity profile than **7e**.
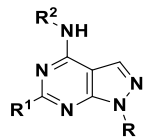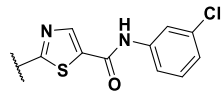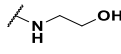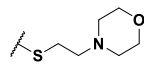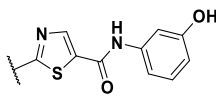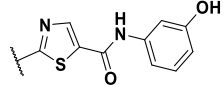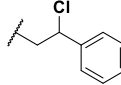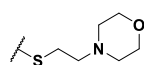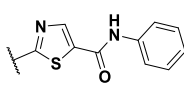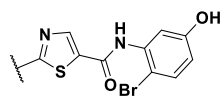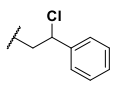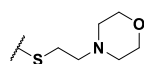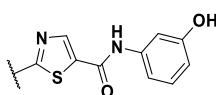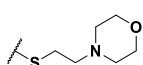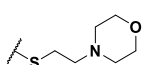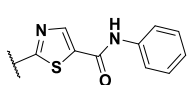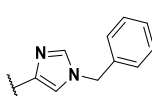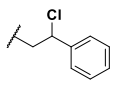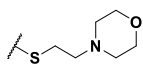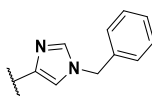
To better understand the physicochemical properties of these derivatives and investigate the discrepancy between the enzymatic and cell activity, the ADME properties of **7a,c-h** were studied *in silico* and *in vitro*. Both predicted (SwissADME) and experimental (thermodynamic) aqueous solubility were determined (Table 3). Predicted logS data highlighted the hydrophobic character of tested derivatives, especially for the C6 unsubstituted compounds **7g,h** (logS values of −8.76 and −8.17, respectively), followed by morpholino derivatives **7a,c,d,e**, which showed logS values of −6.64, −6.27, −6.80, −6.42, respectively. Finally, **7f** resulted a moderately soluble compound (logS = −5.32). On the other hand, the experimental data obtained from thermodynamic water solubility assay confirmed the apolar character of **7a,d,e,g,h**. Indeed, their solubility could not be determined experimentally because the values were below their intrinsic limit of quantification (LoQ) expressed as μg/mL. Moreover, **7c** resulted in a low water solubility (logS = −7.25, corresponding to 0.03 μg/mL). Finally, **7f** showed a logS value of −7.57 (corresponding to 0.01 μg/mL), which allowed to classify **7f** as a poor soluble compound.

Furthermore, the ability of compounds to cross phospholipid bilayers has been investigated by the Parallel Artificial Membrane Permeability (PAMPA) assay (Table 3). When incubated in the presence of an artificial lipidic membrane made of a phosphatidylcholine (PC) solution, most derivatives showed suboptimal apparent permeability (P$_{app}$), including **7c-f** (P$_{app}$ ≤ 0.10 • 10^{-6} cm/s). Compounds **7c-f** showed a higher affinity towards hydrophilic compartments which limits their ability to cross the hydrophobic bilayer. Furthermore, the C6 unsubstituted derivative **7h** showed sub-optimal permeability, probably due to the presence of the phenolic group. Compound **7a** demonstrated its ability to overcome physical membranes with P$_{app}$ of 1.6 • 10^{-6} cm/s, confirming the hypothesis that the introduction of phenolic groups led to decreased P$_{app}$ values. Finally, **7g** demonstrated the best ability to cross PC bilayer with an apparent permeability value higher than 10^{-5} cm/s.

According to preliminary solubility and permeability data, **7c** resulted a low water soluble derivative unable to cross biological membranes efficiently by passive diffusion. Its unfavourable ADME properties may be responsible for the low antiproliferative activity, thus affecting the achievement of the intracellular target.
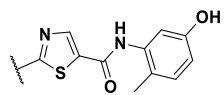
Furthermore, on the basis of the water solubility and P$_{app}$ data obtained, and according to the Biopharmaceutics Classification System's (BCS), **7g** could be classified within BCS class II [compound endowed

Table 1
Enzymatic activity of aminothiazoles **7a-h** and imidazoles **8a,b** towards Src.

Compd	R	R^1	R^2	c-Src IC$_{50}$ (nM) [a]	Inhibition % 10 µM
7a	CH$_3$			134 ± 14	92
7b	CH$_3$			ND	11
7c	CH$_3$			24 ± 4	99
7d	CH$_3$			258 ± 25	90
7e	CH$_3$			0.7 ± 0.1	100
7f	CH$_3$			2.5 ± 1.4	100
7g		H		600 ± 127	91
7h		H		74 ± 14	95
8a	CH$_3$			1000 ± 100	75
8b		SCH^3		ND	25
Dasatinib				20	100

[a] Values are the means of two experiments; ND = Not Determined.

with high permeability (P$_{app}$ > 10^{-5} cm/s) and low solubility (≤0.01 mg/mL)], while **7a,c-f,h** fall within BCS class IV (compounds characterized by suboptimal solubility and apparent permeability) [28,29].

Considering the possible interactions between compounds and phospholipidic bilayer, the percentage of membrane retention (MR) was also detected. Data reported in Table 3 highlighted that the introduction of the bulky bromine atom on the aromatic ring as in **7d** significantly decreased the MR value (0.51 %) compared to the unsubstituted derivatives **7a**, or **7c** and **7e** (MR of 16.49 %, 3.10 % and 19.02 %, respectively). Finally, **7f-h** showed MR ranging from 6.10 % to 8.36 %. These MR% values could explain the cell activity profile of the most

promising Src inhibitors of the series, *i.e.*, such as **7e,f**. Indeed, they resulted less active on cells than expected on the basis of their enzymatic activity.

Then, compounds were also studied in terms of stability in the presence of human liver microsomes (HLMs) and human plasma (Table 4). When incubated for 1 h with HLM, **7d,e,f** and **7h** resulted stable. Also **7a,c** and **7g** resisted well to the metabolizing action of HLMs (99.80 %, 99.40 %, and 99.04 %, respectively), but underwent a slightly greater degradative action leading to the formation of M$_1$ (the opening of the morpholine moiety in C6) for **7a**, M$_2$ (the aromatic oxidation) for derivative **7c**, and M$_3$ (a dechlorination followed by an oxidation in

Table 2

Antiproliferative activity (IC$_{50}$) of **7a,c-h** against the HCC HepG2 and HUH-7 cell lines, and the cytotoxic profile (CC$_{50}$) of **7e** against the healthy keratinocytes HaCaT and embryonic HEK293 cell line.

Cpd	IC$_{50}$ (µM ± SD)					
	HepG2			HUH-7		
	24 h	48 h	72 h	24 h	48 h	72 h
7a	NA[a]	NA	7.9 ± 2.4	67.61 ± 4.52	33.54 ± 2.56	13.95 ± 1.07
7c	>50	>50	>50	–	–	–
7d	12.02 ± 1.98	7.31 ± 2.09	1.55 ± 1.06	26.54 ± 1.89	13.70 ± 0.99	7.21 ± 1.49
7e	59.64 ± 3.56	13.89 ± 2.54	2.47 ± 0.82	54.68 ± 3.93	28.80 ± 2.05	10.33 ± 1.12
7f	NA	NA	6.52 ± 2.17	NA	48.84 ± 3.92	26.11 ± 1.95
7g	NA	7.46 ± 1.34	3.70 ± 0.97	NA	21.23 ± 1.93	15.31 ± 1.15
7h	87.12 ± 3.56	5.06 ± 1.02	3.19 ± 1.08	NA	22.04 ± 1.22	11.05 ± 0.94
Dasatinib	23.48 ± 2.41	9.54 ± 0.98	7.75 ± 1.26	37.54 ± 1.99	16.27 ± 1.13	12.70 ± 0.77

Cpd	CC$_{50}$[b] (µM ± SD)					
	HaCaT			HEK293		
	24 h	**48 h**	**72 h**	**24 h**	**48 h**	**72 h**
7e	92.75 ± 2.17	22.82 ± 1.25	3.27 ± 0.56	18.52 ± 1.11	6.90 ± 0.88	5.23 ± 1.01
Dasatinib	20.38 ± 1.93	1.35 ± 0.69	0.22 ± 0.09	5.40 ± 0.97	0.89 ± 0.05	0.78 ± 0.08

[a] NA = Not Active (IC$_{50}$ ≥ 100 µM).
[b] CC$_{50}$ = concentration that reduced the proliferation of cells by 50 %. Empty cells mean not determined.

Table 3

In silico and *in vitro* aqueous solubility and passive permeability of **7a,c-h**.

Cpd	Aqueous Solubility Assay			PAMPA Permeability Assay	
	Swiss ADME (predicted)	Thermodynamic (experimental)			
	LogS[a]	µg/mL	LogS[a]	P$_{app}$ 10^{-6} cm/s	MR (%)[b]
7a	−6.64	< LoQ[c]	–	1.61 ± 0.34	16.49 ± 5.52
7c	−6.27	0.03	−7.25	0.10 ± 0.04	3.10 ± 1.02
7d	−6.80	< LoQ[c]	–	<0.10	0.51 ± 0.04
7e	−6.42	< LoQ[c]	–	<0.10	19 0.02 ± 0.80
7f	−5.32	0.01	−7.57	<0.10	7.28 ± 1.23
7g	−8.76	< LoQ[c]	–	12.01 ± 0.79	8.36 ± 1.62
7h	−8.17	< LoQ[c]	–	0.14 ± 0.01	6.1 ± 0.3

[a] Logarithm of solubility (solubility expressed as mol/L).
[b] Membrane retention %. Values represent the mean values of three independent experiments run in triplicate.
[c] Limit of quantification (LoQ) = 0.01 µg/mL.

phenylethyl chain in N1 position) and M$_4$ (the carboxamide hydrolysis followed by the restoring of the corresponding acid) for **7g** (the structures of the metabolites are shown in Fig. S4).

Although all compounds can be classified as stable in the presence of HLMs, results suggested that the higher steric hindrance given by the phenol moiety in comparison to the phenyl ring better protects derivatives from microsomal metabolism. Finally, many derivatives resulted very stable after 24 h of incubation with plasma enzymes (values higher than 94 %, Table 4). The exception was represented by **7g,** whose stability was slightly lower (88.53 %). As a consequence of the high plasma stability, very long half-lives (>24 h) were determined, thus suggesting that compounds may reach their target without degradation by plasma enzymes.

According to the results obtained, **7e** is a c-Src inhibitor with low-

Table 4

In vitro HLM and plasma stability of **7a,c-h.**

Cpd	Stability in HLMs		Plasma Stability	
	% after 1h	Metabolite Formation (%)[a]	% after 24h	T$_{1/2}$[b]
7a	99.80 ± 0.12	M$_1$ = 0.20 ± 0.02	98.31 ± 3.39	>24
7c	99.40 ± 0.82	M$_2$ = 0.60 ± 0.04	ND[c]	
7d	>99.99	–	99.45 ± 1.37	
7e	>99.99	–	>99.99	
7f	>99.99	–	94.49 ± 1.56	
7g	99.04 ± 0.31	M$_3$ = 0.31 ± 0.02 M$_4$ = 0.65 ± 0.01	88.53 ± 2.08	
7h	>99.99	–	>99.99	

[a] M$_1$ = opening morpholine ring (-28 + 2); M$_2$ = + OH (+16); M$_3$ = -HCl + O (-36 + 16); M$_4$ = - aniline + OH (−93 + 17).
[b] Half-life (h) expressed as the amount of time it takes before half of the drug is hydrolyzed/degraded. Empty cells were not determined or not found.
[c] ND = Not Determined.

micromolar activity against the HCC HepG2 cell line, better safety profile toward healthy keratinocyte and embryonic cells than dasatinib, and promising ADME properties - in particular, a high metabolic stability, which is fundamental to ensure the biological efficacy towards HCC. These properties led us to deeper investigate its promising anticancer activity in HepG2 cells.

Results obtained from the colony formation assay highlighted the ability of the c-Src inhibitor 7e to significantly reduce HepG2 cell colony formation (Fig. 5 and Fig. S5). Starting from the concentration of 0.5 µM, about a quarter of the effective concentration, moving to the higher concentrations (1–2 µM) this phenomenon was emphasised with the clonogenic capacity reduced to 40 % and 24 %, respectively. These data confirmed the **7e**'s ability to inhibit HCC cell proliferation in a dose-dependent manner.

Studying cancer cells, it is necessary to determine whether a cell line can (or not) resume its proliferative activity after drug treatment. It is crucial to demonstrate the presence of a 'point of no return' that separates cell damage from cell death, beyond which irreversible damage occurs. To better elucidate the mechanism of **7e**-mediated cell death, HepG2 were treated to check whether the inhibitory effect was reversible or irreversible. The treatments were performed for 24 and 48 h, and
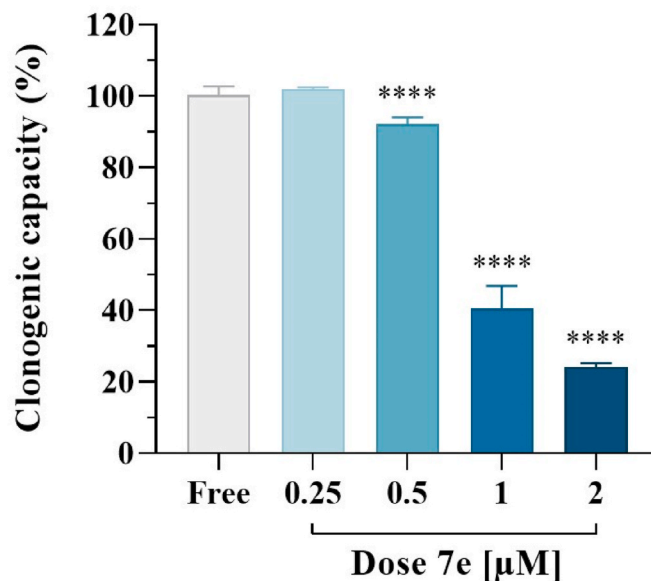

Fig. 5. Clonogenic survival assay of HepG2 cells in response to increasing concentration of **7e** (0.25–0.5-1-2 µM) for 10 days. Values are the means ± SD of n = 3 independent experiments run in triplicate. ****p < 0.001 *vs.* Free (Unpaired Student t-test).

then cells were cultured for further 48 and 24 h, respectively, in a drug-free medium. As reported in Fig. 6, at the endpoint of 72 h (24 + 48 h and 48 + 24 h), was appreciated a general ability of **7e** to induce an irreversible cytotoxic effect, with particularly emphasis at the highest concentrations (10–100 μM). Interestingly, it is important to note that, after 24 h of treatment no cytotoxic effects occurred at both 0.1 and 1 μM, but some irreversible cell-death mechanism was definitely induced since after further 48 h of drug-free treatment a drop of almost 15 % was detected in HCC cell viability.

Since metastasis remains one of the major challenges in the fight against HCC [30], the effect of potential drugs such as **7e** on the migration of these cells was studied. The experiments were conducted exploiting the T-Scratch assay (Fig. 7). While the free samples showed between 40 and 90 % wound closure over the course of the experiment, a general slowing of the closure phenomenon was observed once the cells were in contact with **7e**. As expected, wound closure was affected by the drug concentration; in fact, the trend was less evident at the lowest dose of 0.25 μM, although the closure of the monolayer decreased significantly after 72 h (approaching 70 % wound closure). Increasing the dose to 0.5-1-2 μM showed almost similar behaviour. In fact, compound **7e** suppressed healing, leaving more than 70 % of the wound open at 24 h and almost 40 % after 72 h of treatment. This suggests that **7e** can inhibit the horizontal migration ability of HepG2 cells at the early stage of drug stimulation and is sustained over time (72 h), albeit with decreased inhibition rates.

To investigate whether compound **7e**-induced cell death included aspects of apoptosis, such as DNA fragmentation leading to DNA loss and effects on cell cycle progression, flow cytometry-based cell cycle analyses were performed by exposing HepG2 cells to compound **7e** at its IC_{50} concentration for 72 h. As reported in Fig. 8, a significant accumulation of HepG2 hypodiploid cells in the sub G0/G1 phase was recorded (+44.1 %, p = 0.0005 vs. control), accompanied by a significant decrease in those in the G0/G1 phase (−10.4 %, p < 0.0001 vs. control), indicating apoptotic cell death induced by **7e**. Alongside the rise in DNA fragmentation-afflicted cells, HepG2 cellular proliferation cells was arrested in the S and G2/M phase (+25.2 %, p = 0.030 vs.
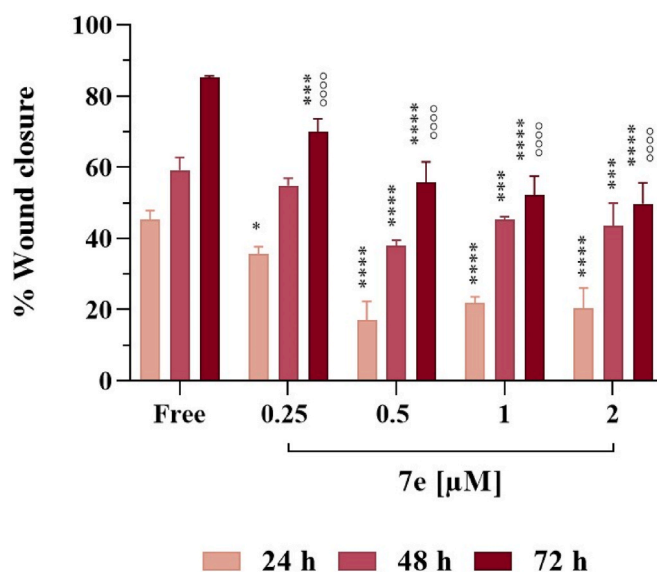
Fig. 7. Effect of compound **7e** on HCC cell migration. After scratching, HepG2 cells were treated with increasing concentrations of compound **7e** for 24-48-72 h. Results were obtained from *n* = 3 independent experiments, and values reported as the means ± SD. The statistical analyses were performed to determine significances with two-way ANOVA followed by Dunnett's multiple comparison test. 0.25 μM: *p = 0.0227; 0.5-1-2 μM: ****p < 0.0001 vs. free at the same timepoint (24 h). 0.5 μM: p < 0.0001; 1–2 μM: ***p = 0.0008–0.0002 vs. free at the same timepoint (48 h). 0.25 μM: ***p = 0.0003; 0.5-1-2 μM: ****p < 0.0001 vs. free at the same timepoint (72 h). 0.25–0.5-1-2 μM at 72 h: p < 0.0001 vs. the same concentration at 24 h.

control and +38.5 %, p < 0.0001 vs. control, respectively), suggesting that some DNA breakage may have occurred during the DNA replication that then led to an incomplete cell cycle.
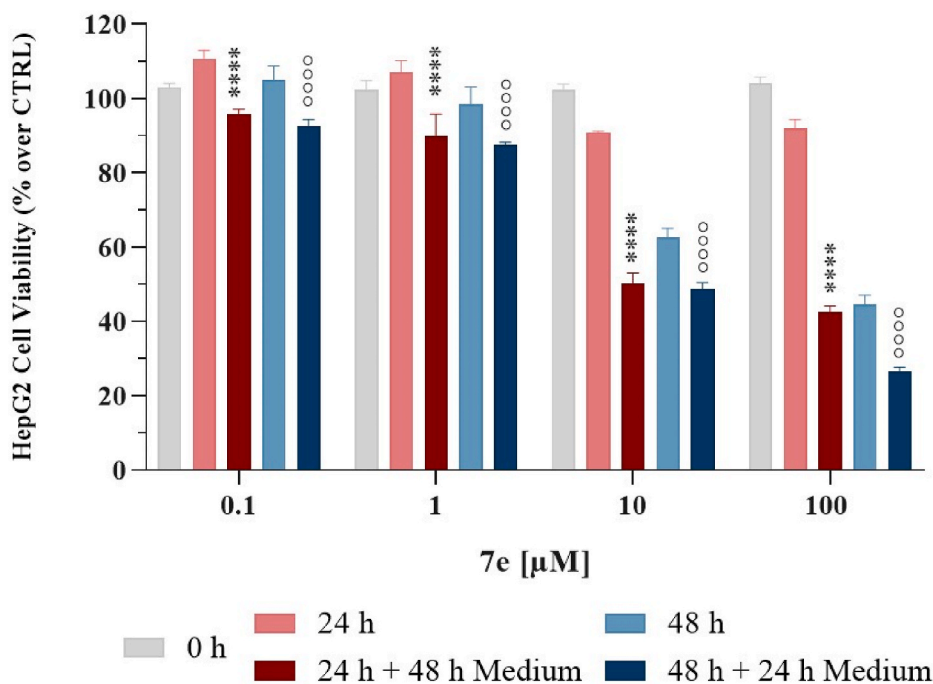
Fig. 6. Irreversible cytotoxic effect of **7e** on HepG2 HCC cell line. Cells were treated with increasing concentrations of **7e** for 24 h (24 h, light-red column) and 48 h (48 h, light-blue column) then incubated for 48 h and 24 h with fresh, drug-free medium (24 h + 48 h medium, dark-red column, and 48 h + 24 h medium, dark-blue column). Values are the means ± SD of *n* = 3 independent experiments run in triplicate. ****p < 0.001 vs. 24 h at the same concentration, and p < 0.001 vs. 48 h at the same concentration (ANOVA followed by Tukey's multiple comparison test).
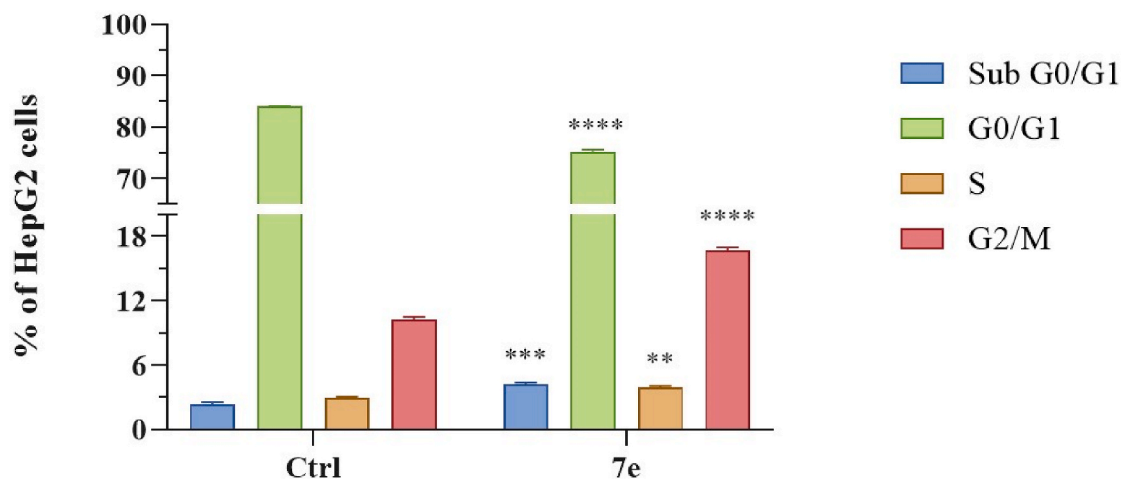
Fig. 8. Compound **7e**-mediated effect on the HCC HepG2 cell cycle. Cells were treated with the IC_{50} value for three days. Percentages of cells in sub G0/G1 (blue bar), G0/G1 (green bar), S (orange bar), and G2/M (red bar) phases are reported as the means $\pm$ SD of $n = 3$ independent experiments run in triplicate. ***p = 0.0005, ****p < 0.0001, and **p = 0.0030 *vs.* ctrl, same cell-cycle phase (Unpaired Student t-test).

3. Conclusion

Starting from an *in-house* pyrazolo[3,4-*d*]pyrimidine SI192 active as c-Src and c-Abl inhibitor, we applied a molecular hybridization approach to design a new generation of derivatives comprised of the pyrazolo-pyrimidine scaffold and molecular portions of an approved TKI. The synthesized compounds were evaluated in a cell-free assay as c-Src inhibitors. The most promising Src inhibitor **7c** was in turn used to design next-generation compounds with a better binding profile based on a hit optimization protocol comprised of molecular modeling and on-paper rational design. As a result, a few nanomolar Src inhibitors active in an HCC *in vitro* model were identified. In particular, **7d-f** showed IC_{50} values of 258, 0.7, and 2.5 nM, respectively, toward Src, and IC_{50} values of 1.55, 2.47, and 6.52 μM, respectively, on the HCC HepG2 cell line after 72 h of treatment. When tested against the HUH-7 cells, **7d-f** confirmed a time- and dose-dependent but worsened antiproliferative activities compared to the HepG2 cells, probably due to the lower c-Src expression. From the biological data **7e** resulted one of the most interesting compounds of the series, thus we evaluated its cytotoxic profile against healthy keratinocytes and embryonic cells. The investigation of the ADME properties of these compounds allowed us to shed light on their physicochemical properties and the discrepancy between enzymatic and cell activity. Lastly, considering the preliminary biological and pharmacokinetic data, **7e** was further characterized evaluating its biological effect on HepG2. Compound **7e** caused permanent cytotoxicity, significantly decreased cellular invasion, and increased the number of cells exhibiting DNA fragmentation, possibly as a result of apoptosis. Overall, this study led to the identification of **7e** which deserves further investigation as a promising TKI in cancer therapies. In particular, a formulation study could be an efficient approach to overcoming the high percentage of membrane retention making the compound available for cell absorption.

4. Experimental section

4.1. Chemistry

All commercially available chemicals were used as purchased. DCM was dried over sodium hydride, THF was dried over Na/benzophenone prior to use, while anhydrous DMF was bought. Anhydrous reactions were run under a positive pressure of dry N_2 or argon. TLC was carried out using Merck TLC plates silica gel 60 F254. Chromatographic purifications were performed on columns packed with Merk 60 silica gel, 23–400 mesh, for flash technique. ^{1}H NMR and ^{13}C NMR spectra were recorded on a Bruker Avance DPX400 (at 400 MHz for ^{1}H and 101 MHz for ^{13}C). Chemical shifts are reported relative to tetramethylsilane at 0.00 ppm. Mass spectra (MS) data were obtained using an Agilent 1100 LC/MSD VL system (G1946C) with a 0.4 mL/min flow rate using a binary solvent system of 95:5 methanol/water. UV detection was monitored at 254 nm. MS were acquired in positive and negative mode scanning over the mass range 50–1500. The following ion source parameters were used: drying gas flow, 9 mL/min; nebulizer pressure, 40 psig; drying gas temperature, 350 °C. All target compounds possessed a purity of ≥95 % as verified by an Agilent 1260 Infinity HPLC-DAD.

4.1.1. Ethyl 5-amino-1-methyl-1H-pyrazole-4-carboxylate (10)

To a solution of **9** (7.00 g, 0.041 mol) in absolute ethanol (30 mL), methyl hydrazine (1.91 g, 0.041 mol) was added and the reaction mixture was stirred for 8 h at reflux. After cooling, the solvent was removed under reduced pressure and the crude was purified by flash chromatography using a gradient of DCM/MeOH (99:1 to 96:4) as eluent to obtain the intermediate **10** as a yellow pale solid. Yield: 73 %. ^{1}H NMR (400 MHz, DMSO-d_6) δ 7.39 (s, 1H), 6.16 (s, 2H), 4.14 (q, $J = 7.0$ Hz, 2H), 3.51 (s, 3H), 1.22 (t, $J = 7.0$ Hz, 3H). MS: 170.2 m/z $[M+1]^+$.

4.1.2. Ethyl 5-(3-benzoylthioureido)-1-methyl-1H-pyrazole-4-carboxylate (11)

Ethyl 5-amino-1-methyl-1*H*-pyrazole-4-carboxylate **10** (5.70 g, 0.034 mol) was dissolved in dry THF (30 mL) and benzoyl isothiocyanate (6.32 g, 0.039 mol) was added dropwise. The reaction mixture was stirred for 6 h at reflux and, after cooling, it was concentrated *in vacuo*. The residue was resolubilized in DCM and triturated with P.E., then filtered on Gooch obtaining **11** as a white solid. Yield: 85 %. ^{1}H NMR (400 MHz, CDCl$_3$) δ 10.6 (bs, 1H), 9.33 (s, 1H), 7.97–7.87 (m, 2H), 7.72–7.63 (m, 1H), 7.59–7.55 (m, 2H), 7.25 (s, 1H), 4.30–4.25 (m, 2H), 3.87 (s, 3H), 1.32–1.28 (m, 3H). MS: 331.0 m/z $[M - 1]^-$.

4.1.3. 6-Mercapto-1-methyl-1H-pyrazolo[3,4-d]pyrimidin-4-ol (12)

Ethyl 5-(3-benzoylthioureido)-1-methyl-1*H*-pyrazole-4-carboxylate **11** (10.23 g, 0.057 mol) was suspended in 2 N NaOH (80 mL) and the reaction mixture stirred for 5 h at reflux. Then, the limpid solution was cooled into an ice-bath and acetic acid was added dropwise to form a white precipitate. The solid compound was filtered on Gooch and washed with toluene to remove the excess of acetic acid obtaining **12** as a white solid. Yield: 88 %. ^{1}H NMR (400 MHz, DMSO-d_6) δ 11.12 (bs, 1H), 10.31 (bs, 1H), 7.85 (s, 1H), 3.82 (s, 3H). MS: 180.1 m/z $[M - 1]^-$.

4.1.4. 1-Methyl-6-((2-morpholinoethyl)thio)-1H-pyrazolo[3,4-d] pyrimidin-4-ol (13)

To a solution of 6-mercapto-1-methyl-1*H*-pyrazolo[3,4-*d*]pyrimidin-4-ol **12** (1.02 g, 0.011 mol) in DMF (10 mL), NaOH (0.356 g, 0.018 mol) previously dissolved in EtOH (10 mL) was added dropwise. Then, chloroethyl morpholine hydrochloride (1.035 g, 0.011 mol) was added and the reaction was stirred for 8 h at reflux. After cooling at rt, the solution was concentrated under vacuum and water was added. The crude was extracted with EtOAc (3 × 50 mL), then the organic layer was washed with LiCl 5 % solution (3 × 60 mL), brine, dried with Na_2SO_4, and concentrated under reduced pressure. The residue was crystallized in diethyl ether obtaining the **13** as a white solid. Yield: 64 %. ^{1}H NMR (400 MHz, CDCl_3) δ 10.21 (bs, 1H), 7.97 (s, 1H), 3.91 (s, 3H), 3.84 (m, 4H), 3.29 (m, 2H), 2.82 (m, 2H), 2.61 (m, 4H). MS: 294.2 m/z [M − 1]⁻.

4.1.5. 4-(2-((4-Chloro-1-methyl-1H-pyrazolo[3,4-d]pyrimidin-6-yl)thio) ethyl)morpholine (14)

The Vilsmeier complex, previously prepared from fresh distilled $POCl_3$ (3.89 g, 0.025 mol) and dry DMF (1.85 g, 0.025 mol) at 0 °C, was added into a solution of **13** (0.750 g, 0.025 mol) in dry $CHCl_3$ (25 mL) and the reaction mixture was stirred for 4 h at reflux. After cooling at rt, water was added and the crude was extracted with $CHCl_3$ (3 × 40 mL). The organic layer was washed with LiCl 5 % solution (3 × 50 mL) and brine, then dried with Na_2SO_4, and concentrated under reduced pressure. The cude was purified by flash chromatography using DCM/MeOH (95:5) as eluent to obtain **14** as a white solid. Yield: 55 %. ^{1}H NMR (400 MHz, CDCl_3) δ 7.96 (s, 1H), 4.01 (s, 3H), 3.70 (m, 4H), 3.35 (t, J = 7.0 Hz, 2H), 2.74 (t, J = 7.0 Hz, 2H), 2.56 (m, 4H). MS: 314.3 m/z [M+1]⁺.

4.1.6. 1-Methyl-6-(methylthio)-1H-pyrazolo[3,4-d]pyrimidin-4-ol (17)

To a solution of 6-mercapto-1-methyl-1*H*-pyrazolo[3,4-*d*]pyrimidin-4-ol **12** (2.03 g, 0.011 mol) in THF (30 mL), iodomethane (7.90 g, 0.056 mol) was added dropwise. The reaction mixture was stirred for 12 h at reflux, then, after cooling at rt, the white precipitate was collected by filtration on Gooch. Trituration using toluene gave **17** as a white solid. Yield: 87 %. ^{1}H NMR (400 MHz, DMSO-*d*₆) δ 10.18 (bs, 1H), 7.93 (s, 1H), 3.90 (s, 3H), 2.55 (m, 3H). MS: 195.1 m/z [M − 1]⁻.

4.1.7. 4-Chloro-1-methyl-6-(methylthio)-1H-pyrazolo[3,4-d]pyrimidine (18)

The Vilsmeier complex, previously prepared from fresh distilled $POCl_3$ (5.86 g, 0.038 mol) and dry DMF (2.79 g, 0.038 mol) at 0 °C, was added into a solution of **17** (0.750 g, 0.004 mol) in dry $CHCl_3$ (20 mL) and the reaction mixture stirred for 4 h at reflux. After cooling at rt, water was added and the crude product was extracted in $CHCl_3$ (3 × 40 mL). The organic layer was washed with LiCl 5 % solution (3 × 50 mL) and brine, then dried with Na_2SO_4, and concentrated under reduced pressure. The cude was purified by flash chromatography using P.E./ EtOAc (8:2) as eluent to obtain **18** as a white solid. Yield: 91 %. ^{1}H NMR (400 MHz, CDCl_3) δ 7.85 (s, 1H), 3.88 (s, 3H), 2.51 (m, 3H). MS: 215.6 m/z [M+1]⁺.

4.1.8. N-(3-hydroxyphenyl)-2-((1-methyl-6-(methylthio)-1H-pyrazolo [3,4-d]pyrimidin-4-yl)amino)thiazole-5-carboxamide (19)

Compound **19** was synthesized according to the general procedure reported for derivatives **7a-e,g,h**. Yield: 82 % ^{1}H NMR (400 MHz, DMSO-*d*₆) δ 12.85 (bs, 1H), 10.08 (bs, 1H), 9.47 (bs, 1H), 8.48–8.40 (m, 2H), 7.35 (s, 1H), 7.22–7.18 (m, 2H), 6.51–6.48 (m, 1H), 3.95 (s, 3H), 2.53 (s, 3H). MS: 412.2 m/z [M − 1]⁻.

4.1.8.1. General procedure for preparation of 7a-e,g,h. To a black solution of Pd_2(dba)₃ (35 mg, 0.038 mmol) and Xantphos (22 mg, 0.038 mmol) in dry 1,4-dioxane (5 mL), the suitable compound (**14** or **20a**, 0.166 mmol) was added and the mixture was stirred for about 30 min at rt. After a while, solution color change to black/orange, K_2CO_3 (70 mg,

0.508 mmol) and the suitable aminothiazole chain **15a-e** (0.228 mmol) were added, and the mixture was stirred for about 4 h at reflux. The reaction was cooled at rt and palladium was filtered on a pad of Celite. The crude was purified by flash chromatography using a proper gradient mixture of DCM/MeOH (99.5:0.5 to 97:3) as eluent and subsequent crystallization in MeOH afforded the desired compounds **7a-e,g,h** as white solids.

4.1.8.1.1. 2-((1-Methyl-6-((2-morpholinoethyl)thio)-1H-pyrazolo [3,4-d]pyrimidin-4-yl)amino)-N-phenylthiazole-5-carboxamide (7a). Yield: 66 %. ^{1}H NMR (400 MHz, CDCl_3) δ 9.19 (bs, 1H), 8.21 (s, 1H), 8.05 (s, 1H), 7.55 (d, J = 7.8 Hz, 2H), 7.16 (t, J = 7.8 Hz, 2H), 6.93 (t, J = 7.8 Hz, 1H), 3.82 (s, 3H), 3.58–3.56 (m, 4H), 3.31 (t, J = 7.1 Hz, 2H), 2.63 (t, J = 7.1 Hz, 2H), 2.43–2.40 (m, 4H). ^{13}C NMR (100 MHz, CDCl_3) δ 168.17, 161.78, 160.12, 154.07, 150.15, 140.46, 138.53, 132.39, 128.68, 123.90, 120.48, 99.19, 66.81, 57.82, 53.45, 33.66, 27.84. MS: 495.0 m/z [M − 1]⁻.

4.1.8.1.2. N-(3-Chlorophenyl)-2-((1-methyl-6-((2-morpholinoethyl) thio)-1H-pyrazolo[3,4-d]pyrimidin-4-yl)amino)thiazole-5-carboxamide (7b). Yield: 45 %. ^{1}H NMR (400 MHz, DMSO-*d*₆) δ 10.88 (bs, 1H), 10.32 (bs, 1H), 8.36–8.32 (m, 2H), 7.89 (s, 1H), 7.63 (d, J = 8.0 Hz, 1H), 7.38 (t, J = 8.0 Hz, 1H), 7.14 (d, J = 8.0 Hz, 1H), 3.92 (s, 3H), 3.59–3.57 (m, 4H), 3.42–3.40 (m, 2H), 2.72–2.70 (m, 2H), 2.52–2.49 (m, 4H). ^{13}C NMR (100 MHz, DMSO-*d*₆) δ 167.8, 161.9, 160.3, 154, 150.2, 141.2, 140.8, 133.5, 132.5, 130.9, 128.6, 123.7, 119.9, 118.7, 99.2, 66.7, 57.8, 53.5, 34.0, 27.8. MS: 530.2 m/z [M − 1]⁻.

4.1.8.1.3. N-(3-hydroxyphenyl)-2-((1-methyl-6-((2-morpholinoethyl) thio)-1H-pyrazolo[3,4-d]pyrimidin-4-yl)amino)thiazole-5-carboxamide (7c). Yield: 59 % ^{1}H NMR (400 MHz, DMSO-*d*₆) 10.05 (bs, 1H), 9.42 (bs, 1H), 8.37 (d, J = 5.3 Hz, 2H), 7.26 (s, 1H), 7.12 (d, J = 4.7 Hz, 2H), 6.50–6.52 (m, 1H), 3.93 (s, 3H), 3.59 (s, 4H), 3.41 (t, J = 7.2 Hz, 2H), 2.71 (t, J = 7.4 Hz, 2H). ^{13}C NMR (100 MHz, DMSO-*d*₆) δ 167.79, 161.57, 159.95, 158.05, 154.00, 150.30, 140.67, 140.27, 132.55, 129.81, 129.30, 111.30, 107.68, 99.11, 66.62, 57.78, 53.52, 34.05, 27.70. MS: 511.0 m/z [M − 1]⁻.

4.1.8.1.4. N-(2-bromo-5-hydroxyphenyl)-2-((1-methyl-6-((2-morpholinoethyl)thio)-1H-pyrazolo[3,4-d]pyrimidin-4-yl)amino)thiazole-5-carboxamide (7d). Yield: 51 % ^{1}H NMR (400 MHz, DMSO-*d*₆) δ 10.34 (bs, 1H), 10.18 (bs, 1H), 8.37 (s, 1H), 8.34 (s, 1H), 7.52 (d, J = 2.4 Hz, 1H), 7.40 (d, J = 8.7 Hz, 1H), 7.08 (dd, J = 8.7, 2.4 Hz, 1H), 3.91 (s, 3H), 3.57 (t, J = 6.2 Hz, 4H), 3.42–3.37 (m, 2H), 2.68 (t, J = 7.2 Hz, 2H). ^{13}C NMR (100 MHz, DMSO-*d*₆) δ 167.72, 161.82, 160.02, 154.45, 153.94, 150.33, 140.99, 139.63, 132.96, 132.50, 128.83, 112.72, 108.31, 103.69, 99.16, 66.62, 57.79, 53.52, 34.00, 27.69. MS: 590.3 m/z [M − 1]⁻.

4.1.8.1.5. N-(5-hydroxy-2-methylphenyl)-2-((1-methyl-6-((2-morpholinoethyl)thio)-1H-pyrazolo[3,4-d]pyrimidin-4-yl)amino)thiazole-5-carboxamide (7e). Yield: 70 %. ^{1}H NMR (400 MHz, DMSO-*d*₆) δ 9.70 (bs, 1H), 9.29 (bs, 1H), 8.34 (s, 1H), 8.30 (s, 1H), 7.02 (d, J = 8.3 Hz, 1H), 6.80 (d, J = 2.5 Hz, 1H), 6.57 (dd, J = 8.3, 2.5 Hz, 1H), 3.91 (s, 3H), 3.56 (t, J = 5.6 Hz, 4H), 3.40–3.35 (m, 2H), 2.67 (t, J = 7.1 Hz, 2H), 2.45–2.42 (m, 4H), 2.11 (s, 3H). ^{13}C NMR (100 MHz, DMSO-*d*₆) δ 167.73, 161.42, 159.90, 155.83, 153.92, 150.27, 140.51, 136.69, 132.54, 131.25, 128.88, 123.67, 113.58, 99.05, 66.60, 57.77, 53.50, 33.98, 27.65, 17.46. MS: 525.1 m/z [M − 1]⁻.

4.1.8.1.6. 2-((1-(2-Chloro-2-phenylethyl)-1H-pyrazolo[3,4-d]pyrimidin-4-yl)amino)-N-phenylthiazole-5-carboxamide (7g). Yield: 57 %. ^{1}H NMR (400 MHz, Acetone-*d*₆) δ 9.62 (bs, 1H), 8.69 (s, 1H), 8.54 (s, 1H), 8.34 (s, 1H), 7.80 (d, J = 8.0 Hz, 2H), 7.53 (d, J = 8.0 Hz, 2H), 7.33–7.29 (m, 5H), 7.07 (t, J = 8.0 Hz, 1H), 5.69–5.66 (m, 1H), 5.11–5.05 (m, 1H), 4.93–4.88 (m, 1H). ^{13}C NMR (100 MHz, Acetone-*d*₆) δ 159.77, 154.22, 150.75, 139.88, 139.16, 138.29, 132.10, 129.02, 128.77, 128.73, 127.59, 123.72, 120.06, 119.97, 101.35, 60.43, 53.43. MS: 473.0 m/z [M − 1]⁻.

4.1.8.1.7. 2-((1-(2-Chloro-2-phenylethyl)-1H-pyrazolo[3,4-d]pyrimidin-4-yl)amino)-N-(3-hydroxyphenyl)thiazole-5-carboxamide (7h). Yield: 48 %. ^{1}H NMR (400 MHz, DMSO-*d*₆) δ 10.05 (bs, 1H), 9.44 (s,

1H), 8.72 (s, 1H), 8.52 (s, 1H), 8.36 (s, 1H), 7.53–7.50 (m, 2H), 7.36–7.26 (m, 4H), 7.11–7.09 (m, 2H), 6.51–6.47 (m, 1H), 5.68–5.65 (m, 1H), 5.09–5.01 (m, 1H), 4.90–4.83 (m, 1H). ^{13}C NMR (100 MHz, DMSO-d_6) δ 161.54, 159.95, 157.99, 154.71, 153.98, 150.85, 140.21, 138.26, 135.24, 134.86, 133.11, 129.77, 129.16, 127.98, 126.76, 111.30, 107.66, 101.29, 66.02, 53.22. MS: 490.1 m/z [M − 1]⁻.

4.1.8.1.8. 2-((6-((2-Hydroxyethyl)amino)-1-methyl-1H-pyrazolo[3,4-d]pyrimidin-4-yl)amino)-N-(3-hydroxyphenyl)thiazole-5-carboxamide (7f). 3-Chloroperbenzoic acid (23 mg, 0.136 mmol) was added to a solution, precooled at 0 °C, of **19** (25 mg, 0.061 mmol) in dry DCM (5 mL) and dry DMF (5 mL) and the mixture stirred at rt for 2 h. Saturated aqueous solution of NaHCO₃ was added in ice bath dropwise until pH = 7 and the mixture was extracted with EtOAc (3 × 40 mL). Organic phase was dried on Na₂SO₄, filtered and concentrated under reduce pressure. The crude was used in the next step without purification. The resulting mixture was dissolved in DMSO/butan-1-ol 1:2 (6 mL). 4-(2-amino-ethyl)morpholine or ethanolamine (0.146 mmol) was added and the reaction mixture was stirred at reflux for 8 h. Water was added and the product was extracted in EtOAc (5 × 40 mL), washed with brine, dried on Na₂SO₄, filtered and concentrated *in vacuo*. The brown solid was purified by flash chromatography using P.E./Acetone (7:3) as eluent to obtain the desired compound **7f** as white solid. Yield: 43 %. ^{1}H NMR (400 MHz, DMSO-d_6) δ 9.98 (bs, 1H), 9.42 (bs, 1H), 8.32 (s, 1H), 8.15 (s, 1H), 7.26 (s, 1H), 7.13–7.08 (m, 2H), 6.48–6.46 (m, 1H), 4.73 (bs, 1H), 3.75 (s, 3H), 3.62–3.60 (m, 2H). ^{13}C NMR (100 MHz, DMSO-d_6) δ 161.99, 160.10, 157.98, 156.22, 140.95, 140.32, 138.04, 132.32, 129.77, 128.65, 111.19, 107.57, 95.93, 33.46, 29.48, 24.54. MS: 425.3 m/z [M − 1]⁻.

4.1.8.2. General procedure for preparation of 8a,b. The intermediate **14** or **20b** (0.058 mmol) was suspended in absolute ethanol (2 mL) and fresh distilled TEA (11 mg, 0.118 mmol) was added dropwise. Compound **16** (16 mg, 0.086 mmol) was added and the reaction was stirred for 6–8 h at reflux. Then, after cooling to rt, the solution was concentrated under vacuum. Purification by flash chromatography using a gradient of DCM/MeOH (99.5:0.5 to 98:2) led to compounds **8a,b** as white solids.

4.1.8.2.1. N-(1-benzyl-1H-imidazole-4-yl)-1-methyl-6-((2-morpholinoethyl)thio)-1H-pyrazolo[3,4-d]pyrimidin-4-amine (8a). Yield: 45 %. ^{1}H NMR (400 MHz, CDCl₃) δ 9.46 (bs, 1H), 7.81 (s, 1H), 7.56 (s, 1H), 7.44–7.29 (m, 4H), 7.29–7.19 (m, 2H), 5.13 (s, 2H), 3.94 (s, 3H), 3.72 (d, 4H), 3.40–3.27 (m, 2H), 2.82–2.69 (m, 2H), 2.55 (d, 4H). ^{13}C NMR (100 MHz, CDCl₃) δ 168.91, 163.14, 146.97, 139.62, 139.22, 135.99, 134.37, 130.93, 130.77, 129.09, 128.48, 127.25, 66.74, 58.22, 53.43, 51.34, 33.53, 27.63. MS: 272.1 m/z [M+1]⁺.

4.1.8.2.2. N-(1-benzyl-1H-imidazole-4-yl)-1-(2-chloro-2-phenylethyl)-6-(methylthio)-1H-pyrazolo[3,4-d] pyrimidin-4-amine (8b). Yield: 65 %. ^{1}H NMR (400 MHz, CDCl₃) δ 9.59 (bs, 1H), 7.81 (s, 1H), 7.50 (s, 1H), 7.44–7.31 (m, 5H), 7.31–7.17 (m, 5H), 5.54–5.48 (m, 1H), 5.12 (s, 2H), 4.88 (dd, J = 14.0, 8.0 Hz, 1H), 4.77 (dd, J = 14.0, 8.0 Hz, 1H), 2.52 (s, 3H). ^{13}C NMR (100 MHz, CDCl₃) δ 165.35, 161.11, 156.80, 154.72, 152.23 146.97, 139.34, 139.21, 135.99, 134.37, 130.93, 130.77, 129.09, 128.48, 127.25, 98.95, 66.74, 58.96, 52.09, 13.50. MS: 476.4 m/z [M+1]⁺.

4.2. Computational details

Protein preparation. The X-ray structures of the complexes between c-Src and pyrazolo[3,4-*d*]pyrimidine derivatives (pdb entry 4o2p, 3el8, and 4dgg) were prepared by using the Protein Preparation Wizard workflow of the Schrodinger suite. Further details in Supporting Information.

Ligand preparation and molecular docking of 7c and its derivatives. Molecular structures of the inhibitors were sketched in Maestro and prepared in terms of tautomeric and ionization states by using the LigPrep tool. The compounds were finally docked within the receptor grids described in the self-docking section (further details in Supporting Information), with the same docking procedure.

Affinity grid maps. The active conformation of Src in the complex with **7c**, as obtained within the GaMD trajectory, was employed to calculate affinity grid maps with AutoDock (further details in Supporting Information.

4.3. Biology

Chemicals. Reagents and solvents were purchased from Sigma-Aldrich S. r.l. (Milan, Italy) and Carlo Erba Reagents S. r.l (Milan, Italy). Cell culture mediums, fetal bovine serum (FBS), ʟ-glutamine, and penicillin–streptomycin were purchased from Euroclone S. p.A. (Milan, Italy). Milli-Q quality water (Millipore, Milford, MA), acetonitrile (ACN) and formic acid (FA) were used for the chromatographic analyses. Human hepatocarcinoma cell lines (HepG2 and HUH-7) and the embryonic ones (HEK293) were purchased from American Type Culture Collection (ATCC) (Manassas, VA), while HaCaT cells by Professor Federica Pessina from the Department of Molecular and Developmental Medicine (University of Siena, Italy). Dasatinib was purchased from Enamine (Monmouth Junction, NJ). All tested compounds were dissolved in dimethyl sulfoxide (DMSO) as a 20 mM stock solution before use and diluted to final concentration with cell culture medium (see below).

Enzymatic Assays. Recombinant Abl and Src were purchased from Promega. Reactions were performed according to the manufacturer's instructions with minor modifications. Peptide substrates were used at least at twice the concentration of apparent K_m. Src reactions were performed using 500 μM Src-peptide (KVEKIGEGTYGVVYK), 100 μM ATP, and 0.00087 % NP-40. Abl reactions were performed using 50 μM abltide (EAIYAAPFAKKK), 30 μM ATP, and 0.00087 % NP-40. All reactions were performed using 10–50 ng of enzyme and 10 % DMSO in 10 μL of kinase buffer (8 mM MOPS-NaOH pH 7.0, 0.2 mM EDTA, 10 mM MgAc) at 30 °C for 10 min. To avoid peptide adsorbing to the plastic surface, protein low-binding tubes were used. ADP-Glo kinase assay (Promega) was then used to detect kinase activity according to the manufacturer's instructions with minor modifications. In detail, reactions were transferred to white 384 well-plates and stopped by adding 10 μL of ADP-Glo reagent (Promega) for 50 min at rt. A total of 20 μL of detection reagent (Promega) was then added for 30 min and the reaction read using a GloMax Discover microplate reader (Promega). Data were plotted using GraphPad Prism 5.0. IC₅₀ values were obtained according to Equation (1):

$$v = V / \{1 + (I / IC_{50})\} \tag{1}$$

where v is the measured reaction velocity, V is the apparent maximal velocity in the absence of inhibitor, I is the inhibitor concentration, and IC₅₀ is the 50 % inhibitory dose. Compounds tested were assumed to act as fully ATP-competitive inhibitors.

Cell culture and anti-proliferative effects on cell-based assays. Cell-based assays were performed to investigate the efficacy using the hepatocarcinoma HepG2 and HUH-7 cell lines and toxicity profile with the HaCaT and HEK293 cells; all cell lines were cultured in Dulbecco's modified Eagle medium (DMEM). The medium was implemented with 10 % FBS, 2 mM ʟ-glutamine, and 10 000 units/mL penicillin/streptomycin at 37 °C in a 5 % CO₂ atmosphere. To evaluate the anti-proliferative activity of the compounds reported as IC₅₀ (*i.e.,* drug concentration that caused 50 % of cell growth inhibition), HepG2 and HUH-7 cells (selected as representative HCC model with high and low Src expression levels) were seeded at a density of $0.1 × 10^5$ in 96-well plates and treated with increasing concentrations of compounds (0.01–1000 μM) for 24, 48, and 72 h. The final concentration of DMSO used never exceeded 0.5 % v/v, and appropriate controls were always performed in each experiment. To evaluate the potential cytotoxic profile of the

candidates toward healthy cells, reported as CC$_{50}$ (*i.e.*, concentration that reduced the proliferation of cells by 50 %), further investigations were conducted using the nontumoral keratinocytes HaCaT cells and the Human embryonic kidney 293 (HEK293) cells. The protocol applied for the evaluation of the toxicity was the same described above for the antiproliferative assays. For both the kind of experiments, 3-(4,5-dimethylthiazol-2-yl)-2,5-diphenyltetrazolium bromide (MTT) was used to assess cell viability as previously described [17]. Briefly, a 0.5 mg/mL MTT solution in FBS-free culture medium was added to each well, and the plates incubated for 4 h. Afterward, formazan violet crystals were solubilized in isopropanol, and the absorbance was quantified at 570 nm using a Multiskan SkyHigh Microplate Spectrophotometer (Thermo-Fisher, Waltham, MA). Cell viability was expressed as a percentage of DMSO-treated cells (controls), taken as 100 %. IC$_{50}$ and CC$_{50}$ values were calculated by fitting data to a nonlinear regression analysis (sigmoidal log concentration *vs.* normalized response curve; GraphPad Prism 5.04 software, GraphPad Software Inc., San Diego, CA) using at least six points in a concentration range from 0 % to 100 % of the studied effects. Dasatinib has been used as reference compound.

HPLC-UV/MS method. The chromatographic analyses were performed using an Agilent 1260 LC/MSD VL system (G1946C) (Agilent Technologies, Palo Alto, CA) constituted by a vacuum solvent degassing unit, a binary high-pressure gradient pump, a 1260 series UV detector, and an 1100 MSD model VL benchtop mass spectrometer. The Agilent 6130 series mass spectra detection (MSD) single-quadrupole instrument was equipped with the orthogonal spray API-ES (Agilent Technologies. Palo Alto, CA). Nitrogen was used as nebulizing and drying gas. Chromatographic separation was performed using a Phenomenex Kinetex EVO C18 - 100 Å (150 mm × 4.6 mm, 5 μm particle size) at rt and gradient elution with a binary solution was conducted as reported in Table 5.

LC-MS/MS method. A triple quadrupole MSD (Mod. 320-LC) mass spectrometer with an ESI interface, two pumps (212-LC), a vacuum solvent degassing unit, and Varian MS Workstation System Control Vers. 6.9 software comprise the Varian (Varian Inc.) system used for the analyses. With a Kinetex C18 column 100 Å 30 × 2.1 mm and with a particle size of 2.6 μm (Phenomenex, Torrance, CA), chromatographic separation was carried out using gradient elution (Table 6) made of solvent A (H$_2$O) and solvent B (ACN), both acidified with FA 0.1 % v/v. The instrument's specifications were as follows: detector: 1450 V; nebulizing gas: 45.0 psi; desolvation temperature: 300.0 °C; needle: 5700 V; shield: 600 V. The instrument was operated in positive mode. Nebulizer and drying gases made of nitrogen were used in the single reaction monitoring (SRM) technique of analyte detection. Argon was used as the collision gas in the collision cell, and the dissociation was generated by collisions at a pressure of 1.8 mTorr.

The transitions, optimum capillary voltages, and collision energies are provided in Table 7.

Thermodynamic water solubility. An aqueous solution (1 mg/mL) was prepared for each tested derivative by adding Milli-Q water. Solutions obtained were stirred at rt overnight and the resulting suspensions were filtered through a 0.45 μm nylon filters (Acrodisc) The quantifications of

Table 5

Chromatographic parameters adopted for the LC-UV/MS method. [a]The detection was conducted in positive [M]$^+$ mode of ionization.

Time (min)	% Eluent A H$_2$O (FA 0.1%$_{v/v}$)	% Eluent B ACN (FA 0.1%$_{v/v}$)	Flow (μL/min)	Injection volume (μL)	Wavelength nm	Scan Range (m/z)[a]
0–1	95	5	600	10	330	100–2000
15–19	5	95				
20	95	5				

Table 6

Chromatographic parameters adopted for the LC-MS/MS method. [a]The detection was conducted in positive [M]$^+$ mode of ionization.

Time (min)	% Eluent A H$_2$O (FA 0.1%$_{v/v}$)	% Eluent B ACN (FA 0.1%$_{v/v}$)	Flow (μL/min)	Injection volume (μL)
0–1	95	5	200	10
5–9	5	95		
10	95	5		

solubilized compound were performed in triplicate by the LC-MS/MS method described above. Data were analyzed by comparing them with the appropriate calibration curve made of DMSO solutions at known concentrations (0.1–100 μM). The LoQ was assessed as lower than 0.01 μM [31].

PAMPA Assay. The DMSO stock solution of each compound was diluted 1:1 v/v with phosphate buffer (PBS 10 mM, pH 7.4) to obtain donor solutions. Each well of the filter plate was covered with a 1 % w/v L-α-phosphatidylcholine solution (PC) in dodecane used to mimic the gastrointestinal (GI) phospholipidic bilayer and then added with the donor. In the acceptor plate, a mixture solution of DMSO/PBS 1:1 v/v was placed, and the sandwich was incubated at rt for 4 h under gentle shaking. At the end time point, samples were taken from both the upper and the lower plates and analyzed using the LC-UV-MS method described above. Apparent permeability (P$_{app}$, measured in 10^{-6} cm/s) was calculated as previously reported by us [32].

Metabolic stability in human liver microsomes (HLM). Each DMSO compound solution was incubated in the presence of phosphate buffer (PBS 10 mM, pH 7.4), HLM (0.2 mg/mL), and a NADPH solution (in MgCl$_2$ 48 mM), at 37 °C for 60 min under shaking. Then, the metabolizing reactions were stopped by adding cold ACN. After centrifuging and drying the reaction mixes under N$_2$ flow, the quantitative analyses were performed using the UV/LC-MS method previously described. The percentages of the metabolized and unmetabolized compounds were calculated as previously described [24,33].

Plasma Stability. A DMSO stock solution of tested compounds was incubated in presence of human plasma (55.7 μg protein/mL) and HEPES buffer (25 mM, 140 mM NaCl, pH 7.4) at 37 °C under shaking. At selected time points (0, 0.083, 0.25, 0.5, 1, 2, 8, 24 h), samples were treated with cold ACN to stop reactions through protein denaturation, and centrifuged at 5000 rpm for 10 min. The supernatant was analyzed by UV/LC-MS to monitor the amount of unmodified compound. Data were calculated with Excel and plotted using GraphPad Prism 8.0 (GraphPad Software Inc., San Diego, CA). The half-life value (t$_{1/2}$) was calculated with the following formula:

$$t_{1/2} = \frac{0.693}{b}$$

Where b is the slope found in the linear fit of the natural logarithm of the fraction remaining of the parent compound *vs.* incubation time [34].

Mechanism of action studies (clonogenic assay, reversible/irreversible effect, cell-cycle analysis, t-scratch assay). To better elucidate the mechanism of action (MoA) and have a more complete vision about the antiproliferative efficacy of **7e**, we firstly assessed the survival and

Table 7

Optimized SRM transitions and instrument parameters of **7a,d,e-h**.

Cpd	Precursor Ion (m/z)	Product Ion (m/z)	Capillary (eV)	Collision Energy (eV)
7a	496.6	410.1	90	−26.5
7d	591.5	505.8	40	−29.5
7e	526.6	506.0	120	−28.0
7f	426.4	409.0	115	−21.0
7g	475.9	440.2	90	−23.5
7h	491.9	409.1	50	−22.0

proliferative capacity of individual cells by clonogenic assay. Unlike other cell viability assays, including the MTT assay used above for the assessment of IC_{50} and CC_{50} values, the clonogenic assay specifically evaluates the long-term survival and proliferative capacity of cells, which is more relevant to assessing the therapeutic efficacy of anticancer agents. Briefly, HepG2 cells were seeded in 6-well plates (1000 cells/dish) in DMEM 10 % FBS and treated with sub-cytotoxic concentrations of **7e** (0.25–0.5-1-2 μM) in humidified atmosphere for 10 days, the time needed for the control cells to form clones large enough. Colonies (>50 cells) were rinsed with PBS, fixed with methanol and stained with crystal violet solution (0.5 % w/v H_2O/MeOH). Removed the staining solution, dishes were washed with tap water and air-dried. Finally, colonies were counted and photographed (Fig. S5) [35]. Then, we investigated if the cytotoxic effect may be reversible or irreversible; thus, HepG2 cells were seeded and treated with derivative **7e** (concentrations ranging from 0.1 to 100 μM) for 24 and 48 h. At endpoints the plates were washed with PBS and cultured in drug-free DMEM with 10 % FBS for 48-24 h, respectively. The MTT assay was then used to determine cell viability as previously described [17]. To test the inhibitory effect of **7e** on cell migration, HepG2 cells (1×10^5 cells/well) were plated on a 24-well plate until they reached 90 % confluence the next day. The cell layer was then scratched with a sterile p200 pipet tip. After rinsing with warm PBS to remove unattached cells, fresh DMEM containing 1 % FBS and escalating doses (0.25–0.5-2.5–5 μM) of compound **7e** were added to each well. The scratched area was photographed at 10X magnification at defined time points (0, 24, 48, 72 h, Fig. S6). Furthermore, we focused our attention to explore whether compound **7e**-mediated cell death involved some aspects of apoptosis, such as loss of DNA due to DNA fragmentation, as well as effects on cell-cycle progression. To this purpose, using flow cytometry-mediated cell-cycle analyses, compound **7e** at its IC_{50} concentration (around 2 μM) was used to treat HepG2 cells for 72 h. The cells were then treated in accordance with earlier reports [17, 36] Using a FACScan flow cytometer and Cell Quest software v.3.0 (both purchased from BD Biosciences, San Jose, CA, USA), red fluorescence (DNA) was detected through a 563–607 nm bandpass filter (FL2 channel, 10^4 cells/sample). The latter was used to calculate the percentage of cells in the different phases of the cell cycle.

CRediT authorship contribution statement

Salvatore Di Maria: Methodology, Formal analysis. **Raffaele Passannanti:** Methodology, Formal analysis. **Federica Poggialini:** Methodology, Formal analysis. **Chiara Vagaggini:** Methodology, Formal analysis. **Alessia Serafinelli:** Formal analysis. **Elena Bianchi:** Formal analysis. **Paolo Governa:** Formal analysis. **Lorenzo Botta:** Writing – review & editing. **Giovanni Maga:** Writing – review & editing. **Emmanuele Crespan:** Methodology, Data curation. **Fabrizio Manetti:** Writing – review & editing. **Elena Dreassi:** Writing – review & editing, Supervision. **Francesca Musumeci:** Writing – review & editing, Writing – original draft. **Anna Carbone:** Writing – review & editing, Writing – original draft. **Silvia Schenone:** Writing – review & editing, Conceptualization.

Declaration of competing interest

The authors declare the following financial interests/personal relationships which may be considered as potential competing interests:

Emmanuele Crespan reports financial support was provided by Italian Association for Cancer Research. Emmanuele Crespan reports financial support was provided by MIUR Projects PRIN 2022. Giovanni Maga reports financial support was provided by Italian Association for Cancer Research. Giovanni Maga reports financial support was provided by MIUR Projects PRIN 2022. If there are other authors, they declare that they have no known competing financial interests or personal relationships that could have appeared to influence the work reported in this paper.

Data availability

Data will be made available on request.

Appendix A. Supplementary data

Supplementary data to this article can be found online at https://doi.org/10.1016/j.ejmech.2024.116929.

Abbreviations used

HCC	hepatocellular carcinoma
TKs	tyrosine kinases
TKIs	TK inhibitors
HepG2	human liver cancer cell line
ADME	absorption, distribution, metabolism and excretion
FDA	Food and Drug Administration
FAK	focal adhesion kinase
SAR	structure-activity relationship
GaMD	Gaussian accelerated MD simulations
DMF	N,N-dimethyl formamide
EtOH	ethanol
DCM	dicholoromethane
DMSO	dimethyl sulfoxide
Boc_2O	di-*tert*-butyl dicarbonate
THF	tetrahydrofuran
TEA	triethylamine
m-CPBA	3-chloroperbenzoic acid
P.E.	petroleum ether
EtOAc	ethyl acetate
$POCl_3$	phosphorus oxychloride
CH_3Cl	chloroform
MeOH	methanol
MR%	percentage of membrane retention
HLMs	human liver microsomes

References

[1] A.G. Singal, P. Lampertico, P. Nahon, Epidemiology and surveillance for hepatocellular carcinoma: new Trends, J. Hepatol. 72 (2020) 250–261, https://doi.org/10.1016/j.jhep.2019.08.025.

[2] N.D. Ferrante, A. Pillai, A.G. Singal, Update on the diagnosis and treatment of hepatocellular carcinoma, Gastroenterol. Hepatol. 16 (2020) 506–516.

[3] M.B. Thomas, A.X. Zhu, Hepatocellular carcinoma: the need for progress, J. Clin. Oncol. 23 (2005) 2892–2899, https://doi.org/10.1200/JCO.2005.03.196.

[4] B. Sangro, P. Sarobe, S. Hervás-Stubbs, I. Melero, Advances in immunotherapy for hepatocellular carcinoma, Nat. Rev. Gastroenterol. Hepatol. 18 (2021) 525–543, https://doi.org/10.1038/s41575-021-00438-0.

[5] T.S. Wai Ling Khoo, A. Rehman, J.K. Olynyk, Tyrosine kinase inhibitors in the treatment of hepatocellular carcinoma, in: J.E.E. Tirnitz-Parker (Ed.), Hepatocellular Carcinoma, Codon Publications, Brisbane (AU), 2019. http://www.ncbi.nlm.nih.gov/books/NBK549199/. (Accessed 12 March 2024).

[6] G.K. Abou-Alfa, L. Schwartz, S. Ricci, D. Amadori, A. Santoro, A. Figer, J. De Greve, J.-Y. Douillard, C. Lathia, B. Schwartz, I. Taylor, M. Moscovici, L.B. Saltz, Phase II study of sorafenib in patients with advanced hepatocellular carcinoma, J. Clin. Oncol. 24 (2006) 4293–4300, https://doi.org/10.1200/JCO.2005.01.3441.

[7] C. For D.E. and Research, Regorafenib, FDA, 2023. https://www.fda.gov/drugs/resources-information-approved-drugs/regorafenib. (Accessed 12 March 2024).

[8] C. for D.E. and Research, FDA Approves Cabozantinib for Hepatocellular Carcinoma, FDA, 2019. https://www.fda.gov/drugs/fda-approves-cabozantinib-hepatocellular-carcinoma. (Accessed 12 March 2024).

[9] J.M. Llovet, R.K. Kelley, A. Villanueva, A.G. Singal, E. Pikarsky, S. Roayaie, R. Lencioni, K. Koike, J. Zucman-Rossi, R.S. Finn, Hepatocellular carcinoma, Nat. Rev. Dis. Prim. 7 (2021) 6, https://doi.org/10.1038/s41572-020-00240-3.

[10] W. Tang, Z. Chen, W. Zhang, Y. Cheng, B. Zhang, F. Wu, Q. Wang, S. Wang, D. Rong, F.P. Reiter, E.N. De Toni, X. Wang, The mechanisms of sorafenib resistance in hepatocellular carcinoma: theoretical basis and therapeutic aspects, Signal Transduct. Targeted Ther. 5 (2020) 87, https://doi.org/10.1038/s41392-020-0187-x.

[11] R.H. Alvarez, H.M. Kantarjian, J.E. Cortes, The role of Src in solid and hematologic malignancies: development of new-generation Src inhibitors, Cancer 107 (2006) 1918–1929, https://doi.org/10.1002/cncr.22215.

[12] Y. Ito, H. Kawakatsu, T. Takeda, M. Sakon, H. Nagano, T. Sakai, E. Miyoshi, K. Noda, M. Tsujimoto, K. Wakasa, M. Monden, N. Matsuura, Activation of c-Src gene product in hepatocellular carcinoma is highly correlated with the indices of early stage phenotype, J. Hepatol. 35 (2001) 68–73, https://doi.org/10.1016/s0168-8278(01)00077-0.

[13] A.Y. Chang, M. Wang, Molecular mechanisms of action and potential biomarkers of growth inhibition of dasatinib (BMS-354825) on hepatocellular carcinoma cells, BMC Cancer 13 (2013) 267, https://doi.org/10.1186/1471-2407-13-267.

[14] T. O'Hare, D.K. Walters, E.P. Stoffregen, T. Jia, P.W. Manley, J. Mestan, S. W. Cowan-Jacob, F.Y. Lee, M.C. Heinrich, M.W.N. Deininger, B.J. Druker, In vitro activity of Bcr-Abl inhibitors AMN107 and BMS-354825 against clinically relevant imatinib-resistant Abl kinase domain mutants, Cancer Res. 65 (2005) 4500–4505, https://doi.org/10.1158/0008-5472.CAN-05-0259.

[15] C. Contadini, C. Cirotti, A. Carbone, M. Norouzi, A. Cianciusi, E. Crespan, C. Perini, G. Maga, D. Barilà, F. Musumeci, S. Schenone, Identification and biological characterization of the pyrazolo[3,4-d]pyrimidine derivative SI388 active as Src inhibitor, Pharmaceuticals 16 (2023) 958, https://doi.org/10.3390/ph16070958.

[16] S. Di Maria, F. Picarazzi, M. Mori, A. Cianciusi, A. Carbone, E. Crespan, C. Perini, S. Sabetta, S. Deplano, F. Poggialini, A. Molinari, R. Aronne, E. Maccioni, G. Maga, A. Angelucci, S. Schenone, F. Musumeci, E. Dreassi, Novel pyrazolo[3,4-d] pyrimidines as dual Src/Bcr-Abl kinase inhibitors: synthesis and biological evaluation for chronic myeloid leukemia treatment, Bioorg. Chem. 128 (2022) 106071, https://doi.org/10.1016/j.bioorg.2022.106071.

[17] F. Poggialini, C. Vagaggini, A. Brai, C. Pasqualini, E. Crespan, G. Maga, C. Perini, N. Cabella, L. Botta, F. Musumeci, M. Frosini, S. Schenone, E. Dreassi, Biological evaluation and in vitro characterization of ADME profile of in-house pyrazolo[3,4-d]pyrimidines as dual tyrosine kinase inhibitors active against glioblastoma multiforme, Pharmaceutics 15 (2023) 453, https://doi.org/10.3390/pharmaceutics15020453.

[18] M. Radi, E. Dreassi, C. Brullo, E. Crespan, C. Tintori, V. Bernardo, M. Valoti, C. Zamperini, H. Daigl, F. Musumeci, F. Carraro, A. Naldini, I. Filippi, G. Maga, S. Schenone, M. Botta, Design, synthesis, biological activity, and ADME properties of pyrazolo[3,4-d]pyrimidines active in hypoxic human leukemia cells: a lead optimization study, J. Med. Chem. 54 (2011) 2610–2626, https://doi.org/10.1021/jm1012819.

[19] C. Tintori, A.L. Fallacara, M. Radi, C. Zamperini, E. Dreassi, E. Crespan, G. Maga, S. Schenone, F. Musumeci, C. Brullo, A. Richters, F. Gasparrini, A. Angelucci, C. Festuccia, S. Delle Monache, D. Rauh, M. Botta, Combining X-ray crystallography and molecular modeling toward the optimization of pyrazolo[3,4-d]pyrimidines as potent c-Src inhibitors active in vivo against neuroblastoma, J. Med. Chem. 58 (2015) 347–361, https://doi.org/10.1021/jm5013159.

[20] A. Kostić, S. Jovanović Stojanov, A. Podolski-Renić, M. Nešović, M. Dragoj, I. Nikolić, G. Tasić, S. Schenone, M. Pešić, J. Dinić, Pyrazolo[3,4-d]pyrimidine tyrosine kinase inhibitors induce oxidative stress in patient-derived glioblastoma cells, Brain Sci. 11 (2021) 884, https://doi.org/10.3390/brainsci11070884.

[21] B. Okram, A. Nagle, F.J. Adrián, C. Lee, P. Ren, X. Wang, T. Sim, Y. Xie, X. Wang, G. Xia, G. Spraggon, M. Warmuth, Y. Liu, N.S. Gray, A general strategy for creating "inactive-conformation" abl inhibitors, Chem. Biol. 13 (2006) 779–786, https://doi.org/10.1016/j.chembiol.2006.05.015.

[22] P. Bernadó, Y. Pérez, D.I. Svergun, M. Pons, Structural characterization of the active and inactive states of Src kinase in solution by small-angle X-ray scattering, J. Mol. Biol. 376 (2008) 492–505, https://doi.org/10.1016/j.jmb.2007.11.066.

[23] D. Shukla, Y. Meng, B. Roux, V.S. Pande, Activation pathway of Src kinase reveals intermediate states as targets for drug design, Nat. Commun. 5 (2014) 3397, https://doi.org/10.1038/ncomms4397.

[24] A. Molinari, A.L. Fallacara, S. Di Maria, C. Zamperini, F. Poggialini, F. Musumeci, S. Schenone, A. Angelucci, A. Colapietro, E. Crespan, M. Kissova, G. Maga, M. Botta, Efficient optimization of pyrazolo[3,4-d]pyrimidines derivatives as c-Src kinase inhibitors in neuroblastoma treatment, Bioorg. Med. Chem. Lett 28 (2018) 3454–3457, https://doi.org/10.1016/j.bmcl.2018.09.024.

[25] F. Pontén, K. Uhlen, The human protein atlas—a tool for pathology, J. Pathol. 216 (2008) 387–393, https://doi.org/10.1002/path.2440.

[26] M. Uhlén, L. Fagerberg, B.M. Hallström, C. Lindskog, P. Oksvold, A. Mardinoglu, Å. Sivertsson, C. Kampf, E. Sjöstedt, A. Asplund, I. Olsson, K. Edlund, E. Lundberg, S. Navani, C.A.-K. Szigyarto, J. Odeberg, D. Djureinovic, J.O. Takanen, S. Hober, T. Alm, P.-H. Edqvist, H. Berling, H. Tegel, J. Mulder, J. Rockberg, P. Nilsson, J. M. Schwenk, H. Hamsten, K. von Feilitzen, M. Forsberg, L. Persson, F. Johansson, M. Zwahlen, G. von Heijne, J. Nielsen, F. Pontén, Tissue-based map of the human proteome, Science 347 (2015) 1260419, https://doi.org/10.1126/science.1260419.

[27] The human protein Atlas. https://www.proteinatlas.org/. (Accessed 9 September 2024).

[28] J. Rautio, H. Kumpulainen, T. Heimbach, R. Oliyai, D. Oh, T. Järvinen, J. Savolainen, Prodrugs: design and clinical applications, Nat. Rev. Drug Discov. 7 (2008) 255–270, https://doi.org/10.1038/nrd2468.

[29] R. Samineni, J. Chimakurthy, S. Konidala, Emerging role of biopharmaceutical classification and biopharmaceutical drug disposition system in dosage form development: a systematic review, Turk J Pharm Sci 19 (2022) 706–713, https://doi.org/10.4274/tjps.galenos.2021.73554.

[30] S. Kummar, N.Q. Shafi, Metastatic hepatocellular carcinoma, Clin. Oncol. 15 (2003) 288–294, https://doi.org/10.1016/S0936-6555(03)00067-0.

[31] L. Maresca, E. Crivaro, F. Migliorini, G. Anichini, A. Giammona, S. Pepe, F. Poggialini, C. Vagaggini, G. Giannini, S. Sestini, L. Borgognoni, A. Lapucci, E. Dreassi, M. Taddei, F. Manetti, E. Petricci, B. Stecca, Targeting GLI1 and GLI2 with small molecule inhibitors to suppress GLI-dependent transcription and tumor growth, Pharmacol. Res. 195 (2023) 106858, https://doi.org/10.1016/j.phrs.2023.106858.

[32] S. Cesarini, I. Vicenti, F. Poggialini, M. Secchi, F. Giammarino, I. Varasi, C. Lodola, M. Zazzi, E. Dreassi, G. Maga, L. Botta, R. Saladino, Privileged scaffold decoration for the identification of the first trisubstituted triazine with anti-SARS-CoV-2 activity, Molecules 27 (2022) 8829, https://doi.org/10.3390/molecules27248829.

[33] S. Murthy, M.G. Nizi, M.M. Maksimainen, S. Massari, J. Alaviuhkola, B.E. Lippok, C. Vagaggini, S.T. Sowa, A. Galera-Prat, Y. Ashok, H. Venkannagari, R. Prunskaite-Hyyryläinen, E. Dreassi, B. Lüscher, P. Korn, O. Tabarrini, L. Lehtiö, [1,2,4] Triazolo[3,4-b]benzothiazole scaffold as versatile nicotinamide mimic allowing nanomolar inhibition of different PARP enzymes, J. Med. Chem. 66 (2023) 1301–1320, https://doi.org/10.1021/acs.jmedchem.2c01460.

[34] G. Vignaroli, C. Zamperini, E. Dreassi, M. Radi, A. Angelucci, P. Sanità, E. Crespan, M. Kissova, G. Maga, S. Schenone, F. Musumeci, M. Botta, Pyrazolo[3,4-d] pyrimidine prodrugs: strategic optimization of the aqueous solubility of dual Src/Abl inhibitors, ACS Med. Chem. Lett. 4 (2013) 622–626, https://doi.org/10.1021/ml4000782.

[35] N.A.P. Franken, H.M. Rodermond, J. Stap, J. Haveman, C. van Bree, Clonogenic assay of cells in vitro, Nat. Protoc. 1 (2006) 2315–2319, https://doi.org/10.1038/nprot.2006.339.

[36] E. Chiaino, R. Stella, C. Peggion, M. Micucci, R. Budriesi, L.B. Mattioli, C. Marzetti, F. Pessina, M. Valoti, M. Frosini, Acacia catechu willd. Extract protects neuronal cells from oxidative stress-induced damage, Antioxidants 11 (2022) 81, https://doi.org/10.3390/antiox11010081.